Geomatica 77 (2025) 100069

Contents lists available at ScienceDirect

Geomatica

journal homepage: www.sciencedirect.com/journal/geomatica

Small fires, big gap: High-resolution VIIRS data reveal widespread underestimation of emissions in sub-Saharan Africa

Boris Ouattara [a,*], Michael Thiel [b], Florent Mouillot [c], Frédéric Chevallier [d], Barbara Sponholz [e]

[a] Institute of Climate-Smart Agriculture, Thuenen Institute, Brunswick 38116, Germany
[b] University of Würzburg, Institute of Geography and Geology, Department of Remote Sensing, John Skilton Str. 4a, Würzburg 97074, Germany
[c] UMR CEFE 5175, Centre National de la Recherche Scientifique, Université de Montpellier, Université Paul-Valéry Montpellier, Ecole Pratique des Hautes Etudes, Institut de Recherche pour le Développement, 1919 route de Mende, 34293 Montpellier Cedex 5, France
[d] Laboratoire des Sciences du Climat et de l'Environnement, LSCE/IPSL, CEA-CNRS-UVSQ, Université Paris-Saclay, Paris, France
[e] University of Würzburg, Institute of Geography and Geology, Department of Geomorphology, Am Hubland, Würzburg 97074, Germany

ARTICLE INFO

Keywords:
Biomass burning
Fire emissions
Small fires
Savanna
VIIRS
MODIS
Sub-Saharan Africa

ABSTRACT

Fires across sub-Saharan Africa (SSA) are a dominant source of global carbon emissions, yet their true magnitude remains uncertain due to the limitations of coarse-resolution satellite products. In this study, we developed a high-resolution fire emission inventory prototype for SSA using active fire detections from the VIIRS sensor (375 m) and a top-down approach based on fire radiative power (FRP). Emissions were estimated through the integration of FRP to fire radiative energy (FRE), conversion to dry matter burned using biome-specific combustion coefficients, and application of emission factors for carbon dioxide. A parallel MODIS-based dataset was also produced using the same methodology to isolate sensor-specific effects. To evaluate detection and modelling differences, the VIIRS-based product (VIIRS-EM) was compared against six widely used global fire emission inventories. In addition, a subset of emissions from small fires (defined as FRP < 10 MW) was derived and assessed separately. Over the period 2013–2022, VIIRS-EM estimated average annual carbon emissions of 3.0 Pg C, which is 50–75 % higher than most MODIS-based inventories. Emission hotspots were identified in agricultural and savanna regions, particularly in West and Central Africa. Small fires contributed significantly to early and late fire-season emissions and revealed widespread underestimation in existing products. Our findings underscore the importance of high-resolution detection and FRP-based modelling for capturing the full extent of African fire activity. The VIIRS-EM inventory provides improved spatial and temporal resolution, with implications for atmospheric composition modelling, greenhouse gas accounting, and regional fire policy development.

1. Introduction

Biomass burning plays a critical role in the global carbon cycle, accounting for approximately 5–10 % of annual carbon emissions [54]. Among all regions, sub-Saharan Africa (SSA) stands out as the most fire-active area globally, accounting for up to half of global fire-related carbon emissions [48]. Fire activity across SSA has profound implications for atmospheric composition, terrestrial carbon stocks, regional air quality, and climate dynamics [27,35]. Despite its global importance, sub-Saharan Africa remains one of the regions with the highest uncertainties in fire emission estimates, due to detection limitations and modelling assumptions in existing inventories.

Estimating fire emissions from space typically relies on two main approaches: burned area (BA)-driven models and methods based on fire radiative power (FRP). BA-based inventories estimate emissions by combining mapped burn extent with assumptions about fuel load, combustion efficiency, and emission factors (EFs) [53,54]. While widely used, this method presents substantial limitations, particularly in regions dominated by small and low-intensity fires. Moderate-resolution satellites such as the Moderate-resolution Imaging Spectroradiometer (MODIS; 500–1000 m) often fail to detect short-lived fires or those occurring under cloud cover, in heterogeneous land cover, or with low

* Corresponding author.
E-mail addresses: blou.ouattara@hotmail.com, boris.ouattara@thuenen.de (B. Ouattara).

https://doi.org/10.1016/j.geomat.2025.100069
Received 22 June 2025; Received in revised form 16 August 2025; Accepted 2 September 2025
Available online 4 September 2025

combustion energy [21,8]. These limitations are especially problematic in SSA, where many fires are fragmented or agriculturally driven. Several studies using higher-resolution datasets have demonstrated that small fires can account for over 40 % of total BA and increase regional fire carbon emissions by up to 80 % compared to standard MODIS-based products [48,51].

In addition to detection constraints, BA-based models are limited by their dependency on post-fire surface reflectance changes, which introduces delays and makes them unsuitable for near-real-time applications. They also rely on static or regionally coarse assumptions about fuel availability and combustion efficiency, leading to considerable uncertainty when applied over large and diverse landscapes.

FRP-based methods offer an alternative approach by estimating emissions from the energy radiated by active fires, which is more directly related to fuel consumption. FRP is measured from thermal anomalies detected in satellite imagery and can be integrated over time to produce fire radiative energy (FRE). This approach, when combined with land cover–specific combustion coefficients and EFs, allows for the generation of spatially and temporally explicit emission estimates 1,3, 60]. The Visible Infrared Imaging Radiometer Suite (VIIRS), onboard the Suomi-NPP satellite, provides active fire detections at 375 m resolution with improved sensitivity to low-FRP events compared to MODIS [37, 52].

FRP-based approaches are especially relevant for operational and near-real-time applications. Because active fire data are available within hours of overpass, these methods can support air quality forecasting, smoke dispersion modelling, and fire management decisions [16,30]. Their ability to capture active combustion during the fire event makes them particularly suitable for regions where fire regimes are influenced by rapidly changing vegetation cover, land use activity, or meteorological conditions, such as in SSA.

The primary objective of this study is to develop and evaluate a high-resolution, FRP-based fire emission inventory for SSA covering the period 2013–2022. The approach is based on active fire detections from VIIRS, with emissions estimated through the integration of FRP to FRE, conversion to dry matter burned using land cover–specific combustion coefficients, and application of biome-specific EFs. Emissions are computed at monthly intervals on a 0.1° spatial grid. A MODIS-based counterpart (MODIS-EM) was also produced using the same methodology to allow for sensor-consistent comparisons.

Special emphasis is placed on quantifying emissions from small fires, defined here as those with FRP values below 10 MW. Here we adopt an FRP-based definition (FRP $<$ 10 MW), which characterizes intensity rather than BA. These low-intensity or sub-resolution events are often missed by traditional BA or FRP assimilation products but are prevalent in fragmented landscapes such as cropland and savanna mosaics [34]. To assess the representativeness of our VIIRS-based inventory prototype (VIIRS-EM), we compare it against six widely used global fire emission datasets: GFED4s, GFAS, QFED, FEER, FINN_modis, and FINN_viirs. The comparison focuses on spatial distribution, interannual trends, and seasonal dynamics, and includes an analysis of the relative bias associated with small fire emissions.

2. Materials

2.1. Study area

This study focuses on SSA, defined as the continental region south of approximately 15° N (Fig. 1). The area includes a diversity of fire-prone ecosystems such as tropical savannas, shrublands, dry woodlands, grasslands, and agricultural mosaics [12,15,58]. SSA is a major contributor to global biomass burning emissions, with fires driven primarily by anthropogenic activities including land clearing, residue burning, and pasture management [4,50,65].

Fire activity in SSA is shaped by seasonal climate patterns, particularly the migration of the Intertropical Convergence Zone (ITCZ), which

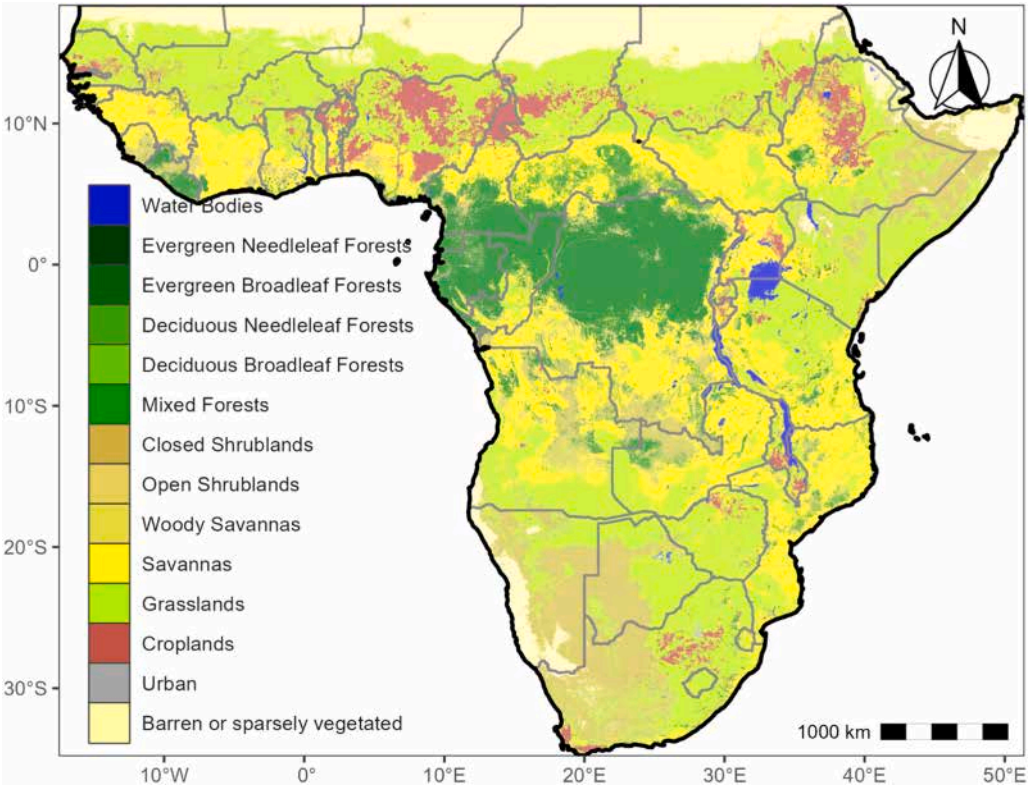

Fig. 1. Geographic extent of the study area covering sub-Saharan Africa with key ecological zones and political boundaries. The two subregions used for analysis, Northern Hemisphere Africa (NHAF) and Southern Hemisphere Africa (SHAF), are delineated for comparative purposes. based on MCD12Q1 (v6.1) for the year 2022 at 500 m resolution, using the University of Maryland (UMD) classification scheme [17].

controls the alternation between dry and wet seasons across hemispheres. In Northern Hemisphere Africa (NHAF), peak fire activity occurs from November to February, while in Southern Hemisphere Africa (SHAF), burning is most intense between May and September [27,49]. These opposing seasonal cycles result in asynchronous fire regimes. For analytical purposes, we distinguish between NHAF and SHAF based on their position relative to the equator.

Most fires in SSA are surface fires occurring in open or semi-open landscapes. Fire behaviour varies with vegetation structure, and fire temperature is generally lower in densely wooded areas where canopy closure suppresses surface fuel availability [33]. Both natural ignitions, such as lightning, and human interventions contribute to fire occurrence across the region. Fire use is strongly embedded in local land-use systems. Communities across SSA rely on fire for multiple purposes, including land preparation, weed and pest control, post-harvest burning, and pasture regeneration [4,6]. These traditional practices influence ecosystem dynamics such as vegetation turnover, soil nutrient cycling, and species composition while also presenting challenges for fire management in the context of land use intensification and climate variability [36,40].

SSA fire emissions influence regional air quality, atmospheric composition, and hydrological processes. Aerosols and trace gases released by biomass burning affect radiation balance, cloud formation, and precipitation. These interactions can create feedbacks that influence future fire activity [35]. Accurate characterization of fire dynamics in SSA is essential for improving emission estimates and informing regional land and fire management policies.

2.2. Active fires

Active fire detections are the primary data source for estimating FRP and subsequent emissions. We used two widely recognized satellite-based products used in operational fire monitoring systems such as EFFIS [9]:

- MODIS Active Fires (MCD14ML, Collection 6)**:** Provides 1 km resolution thermal anomalies from the Terra and Aqua satellites. This product has global coverage and a long temporal record but is known to underdetect small and low-intensity fires due to coarse resolution and sensor limitations [22].
- VIIRS Active Fires (VNP14IMG, Collection 1)**:** Derived from the Suomi-NPP platform, this product offers enhanced spatial resolution (375 m at nadir) and improved sensitivity to low-FRP events, making it more suitable for capturing short-lived and fragmented fires [37,52]. The recently released Collection 2 of the VIIRS Active Fires product [20] provides further enhancements in fire detection, including improved cross-calibration between Suomi-NPP and NOAA-20, as well as refinements to the cloud/snow mask. However, these data were not yet available at the time of writing and were therefore not included in the present analysis. Therefore, all results presented here are based on Collection 1.

Both datasets were processed over the period 2013–2022 using a standardized pre-processing workflow. For MODIS, detections with a confidence level below 50 % were excluded. For VIIRS, we retained only detections classified as “nominal” or “high” confidence based on the categorical flags provided in the VNP14IMG product [44]. Duplicate observations arising from overlapping satellite overpasses were filtered to avoid redundancy. Fire detections were then spatially aggregated to a uniform grid of 0.1° resolution and temporally averaged at daily and monthly scales. Different perimeter delineation approaches for converting fire spots into BA or contiguous fire events can lead to significant differences in fire characterization [7]. Our choice of a standardized gridding workflow ensures methodological consistency with FRP-based emissions estimation. Additional quality control steps included the exclusion of detections not classified as vegetation fires. Specifically, only detections with Type = 0 (presumed vegetation fire) were retained, excluding known sources such as volcanoes (Type = 1), static land sources (Type = 2), and offshore events (Type = 3). This filtering is based on the hot spot type flags provided in the VIIRS and MODIS active fire products. The resulting filtered dataset provided the basis for FRP integration and was subsequently used to estimate emissions following the radiative energy methodology described in Section 3.

2.3. Ancillary data

Land cover classification was used to assign each fire detection to a fire type category, enabling the application of biome-specific combustion coefficients and EFs. We used the MODIS Land Cover Type product (MCD12Q1, Collection 6.1), based on the University of Maryland classification scheme [17]. This product provides annual global land cover at 500 m resolution across 15 land cover classes. For each year of the study period (2013–2022), the corresponding annual land cover map was used to ensure temporal consistency with fire detection data.

Fire pixels were reclassified into generalized fire categories based on the correspondence between MODIS land cover classes and fire types defined by Akagi et al. [1]. These categories include savanna, cropland, tropical forest, shrubland, grassland, and temperate forest, among others. This reclassification allowed for consistent assignment of combustion parameters and reflects the variability in vegetation structure and fuel composition relevant to fire emissions (Table 1).

The combustion coefficient (α) represents the amount of dry matter burned (DMB) per unit of fire radiative energy (in kg MJ^{-1}) and varies by fire type. Values were selected from Akagi et al. [1] and range, for example, from 0.41 kg MJ^{-1} for crop residue fires to 0.90 kg MJ^{-1} for savanna fires. These coefficients were used to convert FRE to DMB as part of the emission modelling process described in Section 3.

Although alternative EF frameworks, such as those proposed by Vernooij et al. [56], offer dynamic emission factor models based on combustion phase or fire season, these were not applied in the current analysis. Instead, the static EFs from Andreae [3] were retained to ensure consistency and comparability with global emission inventories.

3. Methods

We implemented a satellite-based, top-down approach to estimate fire emissions in SSA using active fire detections from VIIRS and MODIS. Our methodology relies on FRP as the primary input and integrates standardized pre-processing, biome-specific combustion coefficients, and EFs application within a gridded framework. The method was used to generate two fire emission products: a VIIRS-based estimate (VIIRS-EM) and a MODIS-based counterpart (MODIS-EM), both using identical computational steps but different input sensors. This structure allows direct comparison of emission outcomes attributable to sensor

Table 1
Correspondence between MODIS land cover classes (MCD12Q1, Collection 6.1; UMD scheme) and fire type categories used for emissions modelling. Conversion factors (kg dry matter burned per MJ) are based on [1], and CO_2 emission factors (in g kg^{-1} of dry matter burned) are taken from [3].

MODIS LULC class (UMD scheme)	Merged fire type category	Conversion factor (kg MJ^{-1})	CO_2 EF (g kg^{-1})
Woody savannas Savannas	Savanna	0.90	1610
Grasslands	Grasslands	0.55	1660
Croplands	Crop residue	0.41	1430
Evergreen broadleaf forests Deciduous broadleaf forests	Tropical forest	1.04	1630
Mixed forests	Temperate forest	0.62	1570
Closed shrublands Open shrublands	Shrubland	0.45	1690

characteristics. In addition to generating full-resolution emissions, we defined a subset of VIIRS-EM restricted to detections with FRP below 10 MW to isolate emissions from low-intensity fires typically missed by moderate-resolution systems. The VIIRS-EM dataset was compared against six widely used global fire emission inventories to assess differences in spatial patterns, total carbon emissions, and representation of small fires. A schematic representation of the full processing chain is presented in Fig. 2. We also computed annual totals of emissions for SSA and its subregions, including NHAF and SHAF, to evaluate decadal trends using a Mann–Kendall test and Sen's slope estimator.

3.1. Computation of fire radiative energy and dry matter burned

We estimated fire emissions using a top-down approach based on FRP derived from VIIRS active fire detections. For each fire detection, instantaneous FRP values from day and night overpasses were processed to calculate FRE, which represents the total radiative output over the burning duration. FRE was computed by integrating FRP over time following the method introduced by [60], and is expressed in megajoules (MJ) (Eq. 1).

The gridding process involved aggregating fire detections to a regular $0.1^\circ \times 0.1^\circ$ spatial grid, consistent with the resolution used for comparison against global fire emission inventories. Within each grid cell, FRP observations from both day and night detections were first averaged separately, then merged to derive a mean daily FRP value. This approach smooths sub-daily fluctuations and reduces noise from isolated short-duration detections, particularly in fragmented agricultural landscapes. Fires detected in both overpasses are typically longer-lived or more intense, while those observed only once may reflect brief or low-FRP activity [52]. Averaging reduces potential overestimation from overlapping or redundant detections and improves spatial coherence in gridded FRE estimates. This value was then temporally integrated over the day to calculate daily FRE per grid cell. The integration step aggregates the instantaneous radiative flux from multiple fire detections, resulting in a spatially consistent and temporally resolved gridded dataset of FRE. This representation allows spatially explicit analysis of fire activity and facilitates emission comparisons with coarser-resolution products.

$$FRE_{i,j} = \left(FRP_{i,j}^{day} + FRP_{i,j}^{night}\right) \times \Delta t \quad (1)$$

Where $FRP_{i,j}^{day}$ and $FRP_{i,j}^{night}$ are the day and night FRP values (in MW) observed in grid cell (i,j), Δt and is the assumed duration of fire activity between overpasses, set to 12 h [30,62].

To convert FRE into biomass consumption, we applied land cover–specific combustion coefficients (α), defined in kg of dry matter burned

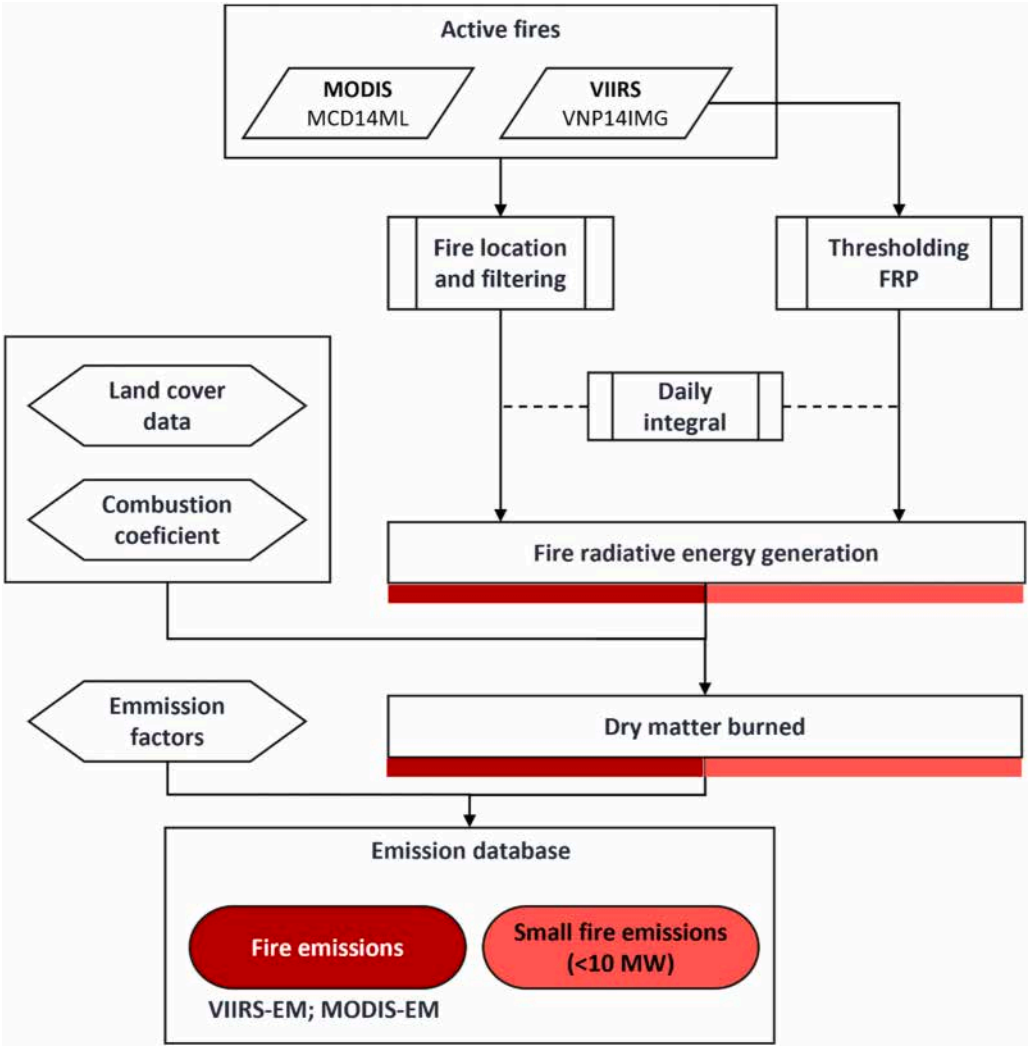

Fig. 2. Overview of the methodological workflow used to generate fire emission estimates for sub-Saharan Africa. The method produces two emission datasets: VIIRS-EM (based on VIIRS detections) and MODIS-EM (based on MODIS detections), both aggregated to a regular 0.1° spatial grid. In addition to generating full-resolution emissions, we defined a subset of VIIRS-EM restricted to detections with FRP below 10 MW to isolate emissions from low-intensity fires.

per megajoule. These coefficients were assigned based on fire type classification derived from annual MODIS MCD12Q1 land cover maps, using the University of Maryland scheme [17]. Each fire pixel was matched to a generalized fire category following the typology in Akagi et al. [1], which includes savanna, cropland, grassland, shrubland, tropical forest, and others. Combustion coefficients ranged from 0.41 kg MJ^{-1} for crop residue fires to 0.90 kg MJ^{-1} for savannas. This stratification improves the accuracy of DMB estimation by accounting for biome-level variability in fuel type and combustion completeness.

In addition to VIIRS-based processing, we developed a parallel MODIS-based emission product (MODIS-EM) using the same FRP-to-biomass methodology. This version relies on 1 km MODIS active fire detections from the MCD14ML product and was designed to enable consistent comparison of emission estimates between sensors. MODIS-EM was processed using the same combustion coefficients, EFs, and aggregation steps described above.

3.2. Emission factor application and CO_2-to-C conversion

To estimate emissions from DMB, we applied fire-type–specific EFs from the global synthesis by Andreae [3]. EFs were expressed in grams of species emitted per kilogram of dry matter burned (g kg^{-1}). For this study, we focused exclusively on carbon dioxide (CO_2), which constitutes the majority of biomass combustion emissions. EFs values for CO_2 ranged from approximately 1450 to 1660 g kg^{-1} , depending on fire type.

Following emission calculation, CO_2 totals were converted to elemental carbon (C) by applying a conversion factor of 3.67, representing the molecular weight ratio between CO_2 and carbon. All emissions were expressed in mass of carbon and aggregated at monthly and 0.1° spatial resolution to support spatial and temporal comparison with global inventories.

3.3. Identification and estimation of small fire emissions

Although our FRP-based method does not require fire size mapping, we performed a targeted classification to isolate emissions originating from small fires. These were defined strictly as fires with FRP below 10 MW, following the nominal lower detection limit of the MODIS fire product [37,52]. This threshold is an intensity-based criterion and should not be confused with burned area. For context, such FRP values are typically associated with relatively low-intensity or short-duration fire events that may correspond to small burned patches (often $<$ 100 ha), which are frequently omitted in moderate-resolution inventories [43].

All VIIRS fire pixels with FRP $<$ 10 MW were flagged and processed using the same FRE-based emission method. The resulting dataset allowed for estimation of emissions from small fires at high spatial and temporal resolution. This subset of VIIRS-EM was used for evaluating the contribution of small fires across SSA and for computing the relative bias of six global fire emission inventories, as shown in Section 4.4. The spatial distribution and quantitative importance of these small fires are discussed in relation to the systematic underestimation observed in MODIS-based inventories, particularly in regions with fragmented agricultural and savanna landscapes.

3.4. Global fire emission inventories

We evaluated our VIIRS-based emission product against six global fire emission datasets commonly used in atmospheric and climate modelling (Table 2). These inventories represent a range of methodological approaches, including FRP-based assimilation, burned-area models, and cluster-based fire detection aggregation.

(1) The Fire Energetics and Emissions Research (FEER) product is an FRP-based inventory developed by NASA that combines MODIS fire detections with regionally tuned emission coefficients [28]. (2) and (3) The Fire INventory from NCAR (FINN v2.5) was evaluated in two configurations: FINN_modis, which uses only MODIS active fires, and FINN_viirs, which integrates both MODIS and VIIRS detections. Both rely on spatial clustering of fire detections to estimate BA at ~1 km resolution. FINN_viirs includes more low-intensity fire events and consequently yields higher emission totals than the MODIS-only version [59]. (4) The Global Fire Assimilation System (GFAS) is an FRP-based emission system developed by the Copernicus Atmosphere Monitoring Service (CAMS). It assimilates MODIS FRP observations in near real time to estimate trace gas and aerosol emissions at a 0.1° resolution [30]. (5) The Global Fire Emissions Database version 4 s (GFED4s) is a burned-area-driven inventory that includes a correction factor to approximate emissions from small fires missed by coarse BA maps [54]. (6) The Quick Fire Emissions Dataset (QFED) is an FRP-based product tuned to reproduce satellite-derived aerosol optical depth patterns, often resulting in higher particulate emissions in regions with dense smoke [10].

Table 2
Global fire emission inventories used for comparison with the prototype VIIRS-based emissions developed in this study.

Inventory	Abbrev.	version	Original spatial resolution	References
Fire Energetics and Emissions Research	FEER	1.0-g1.2	0.1°	[28]
Fire INventory from NCAR	FINN_mod	2.5		[59]
	FINN_viirs		1 km	[59]
Global Fire Assimilation System	GFAS	1.2	0.1°	[30]
Global Fire Emissions Database	GFED4s	4 s	2.5°	[54]
Quick Fire Emissions Dataset	QFED	2.6	0.1°	[10]

At the time of writing, the versions presented in Table 2 reflect the most recent publicly available products. We acknowledge that most of these inventories are actively evolving, with ongoing efforts to improve their ability to represent small, fragmented fires. The comparisons made here are not intended as definitive performance rankings but rather to illustrate key differences in magnitude, spatial patterns, and methodological assumptions relative to our high-resolution, FRP-based prototype. This evaluation provides context for understanding how detection sensitivity and modelling choices influence fire emission estimates.

4. Results

4.1. Higher fire emissions than coarse-resolution models

Our VIIRS-EM inventory yields substantially higher fire emissions for SSA than most existing global emission products (Fig. 3). Over the 2013–2022 period, the average annual carbon emission from VIIRS-EM is approximately 3.0 Pg C, equivalent to 11 100 Tg CO_2 yr^{-1} . This is notably higher than the estimates from MODIS-era inventories. For example, GFED4s yields 0.93 Pg C yr^{-1} , GFAS 0.74 Pg C yr^{-1} , QFED 0.84 Pg C yr^{-1} , FEER 1.44 Pg C yr^{-1} , and FINN_modis 1.37 Pg C yr^{-1} . In contrast, the FINN_viirs inventory, which incorporates VIIRS detections in addition to MODIS, reports a higher value of 3.40 Pg C yr^{-1} (about 13 % above our VIIRS-EM).

These differences reflect a broader pattern: VIIRS-based approaches, which can detect smaller and shorter-lived fires, tend to produce higher fire emission totals than MODIS-only inventories. Across sub-regions, the gap between VIIRS-EM and other inventories varies widely, from as little as + 6 % (relative to FINN_viirs) to as much as + 78 % (relative to GFAS), highlighting the sensitivity of regional totals to detection capability and inventory design. In both NHAF and SHAF, VIIRS-EM exceeds most global inventories by large margins. For example, in NHAF, VIIRS-EM estimates 1.28 Pg C yr^{-1} on average, compared to 0.65

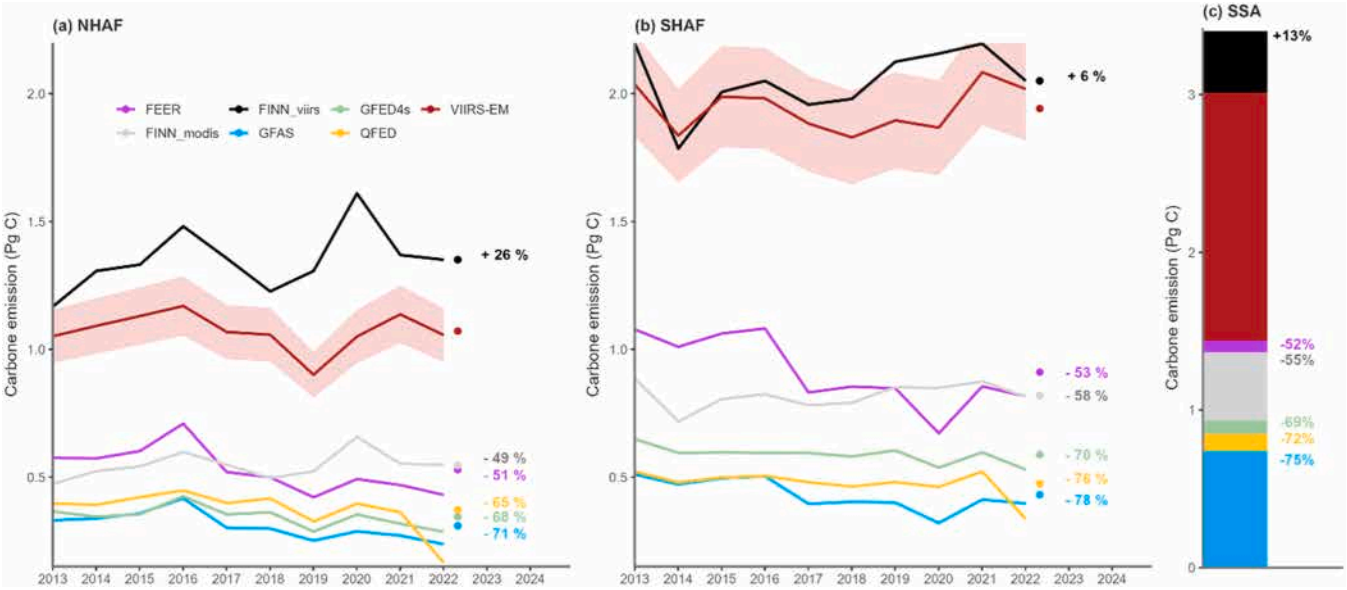

Fig. 3. Annual total fire carbon emissions over 2013–2022 for NHAF (a), SHAF (b), and SSA (c), comparing VIIRS-EM with six global emission inventories. Panels (a) and (b) show time series with shaded envelopes for VIIRS-EM variability and relative bias percentages for each inventory. Panel (c) summarizes the SSA mean over the full period, with bar height showing total emissions and overlaid labels showing average relative bias versus VIIRS-EM. Inventories based on MODIS active fire or burned area (GFED4s, GFAS, QFED, FEER, FINN_modis) are consistently lower than VIIRS-EM, while FINN_viirs (which also uses VIIRS detections) aligns more closely. Units: 1 Pg C = 1 000 Tg C = 10^6 Gg C = 10^9 Mg C = 10^9 t C.

Pg C yr^{-1} for FEER, 0.67 Pg C yr^{-1} for FINN_modis, 0.49 Pg C yr^{-1} for GFED4s, and 0.37 Pg C yr^{-1} for GFAS. The corresponding relative biases in NHAF, using VIIRS-EM as a baseline, are approximately −49 % (GFED4s), −51 % (FEER), −65 % (QFED), −68 % (GFAS), and −48 % (FINN_modis). In SHAF, where total emissions are slightly higher, the biases are similarly large: GFAS underestimates SHAF by −78 %, QFED by −76 %, and GFED4s by −70 %. FEER and FINN_modis are 53–58 % lower than VIIRS-EM. Only FINN_viirs approaches the high totals of VIIRS-EM, coming within 6 % in SHAF and 26 % in NHAF.

When aggregating over the entire SSA domain, VIIRS-EM exceeds all MODIS-based inventories, including QFED, GFAS, GFED4s, FEER, and FINN_modis. These gaps reflect limitations related to coarse spatial resolution and the omission of small fires. We note that we also generated a MODIS-only version of our method (MODIS-EM), which yields intermediate results at 2.69 Pg C yr^{-1} . This version is not shown in Fig. 3 for clarity, but it is informative. The higher estimate from MODIS-EM, relative to other MODIS-based inventories, demonstrates that methodology also influences results. Our approach directly integrates FRP over time and applies biome-specific combustion and emission factors, rather than relying on BA (as in GFED and FEER) or data assimilation with aerosol constraints (as in GFAS and QFED). This allows MODIS-EM to capture more fire activity, particularly from small or short-lived burns that may be underrepresented in other models. The consistently lower totals from standard MODIS-based inventories highlight the importance of both detection resolution and modelling approach in estimating fire emissions.

A statistical analysis of the annual totals reveals a modest but statistically significant decline in fire emissions over the 2013–2022 decade, visible in most inventories including our VIIRS-EM. We estimate a decrease of approximately −1 % per year in SSA fire carbon emissions, with a Sen's slope of −0.013 Pg C yr^{-1} and a Mann–Kendall test indicating statistical significance at the 95 % confidence level ($p < 0.05$), consistent with long-term declines in BA reported by satellite-based studies ([64]; Y. [38]). Our high-resolution emissions remain systematically higher than those from traditional MODIS-based inventories, indicating that a substantial portion of African fire activity has historically been missed. This underestimation persists even in years that exhibit an overall decline, revealing a structural bias related to limited fire detection capability (Figs. 3a, 3b). These findings emphasize the importance of incorporating high-resolution sensors such as VIIRS into fire emissions estimation. Even when using identical methodology, the choice of satellite sensor leads to notable differences: VIIRS-EM totals are typically 10–15 % higher than MODIS-EM, and approximately 50–75 % higher than conventional MODIS-based global inventories on average (Fig. 3c). In some cases, the differences reach a factor of three to four in absolute terms. Improving fire detection capacity can thus alter national and continental carbon budgets by 50–200 %, with direct consequences for climate modelling, emissions reporting, and mitigation planning.

4.2. *Spatial distribution and hotspots*

The spatial patterns in our VIIRS-EM inventory reveal concentrated fire emissions in a limited number of dominant regions across SSA (Fig. 4). The highest emission totals are observed along two broad latitudinal belts. The first is located in the northern tropical savannas of West and Central Africa (5–15° N), where regions such as northern Cameroon, southern Chad, the Central African Republic, South Sudan, and northern Democratic Republic of Congo exhibit dense fire activity. The second major hotspot is situated in the dry woodlands of Southern Hemisphere Africa (5–15° S), encompassing northern Angola, southern DRC, eastern Zambia, and northern Mozambique. These two zones correspond approximately to the Sudanian and Sahelian savannas in the north and the Miombo–Mopane woodlands in the south, both of which are subject to recurrent biomass burning during the dry season.

Elevated emissions also occur in parts of West Africa's agricultural corridor (approximately 0–10° N, 0–10° W), where fragmented smallholder farming leads to extensive patch-burning of fields and fallow areas. In contrast, the humid equatorial forests of the Congo Basin (around 0–5° N, 15–30° E) show limited fire emissions. This is consistent with the bioclimatic suppression of fire in perhumid rainforests and relatively low fire use in these zones, apart from the forest–savanna boundary and areas undergoing deforestation. Similarly, hyper-arid regions such as the southern Sahara (approximately 15–25° N), the Horn of Africa (roughly 5–15° N, 35–50° E), and the Kalahari Desert (around 20–30° S, 15–25° E) exhibit minimal fire activity due to limited

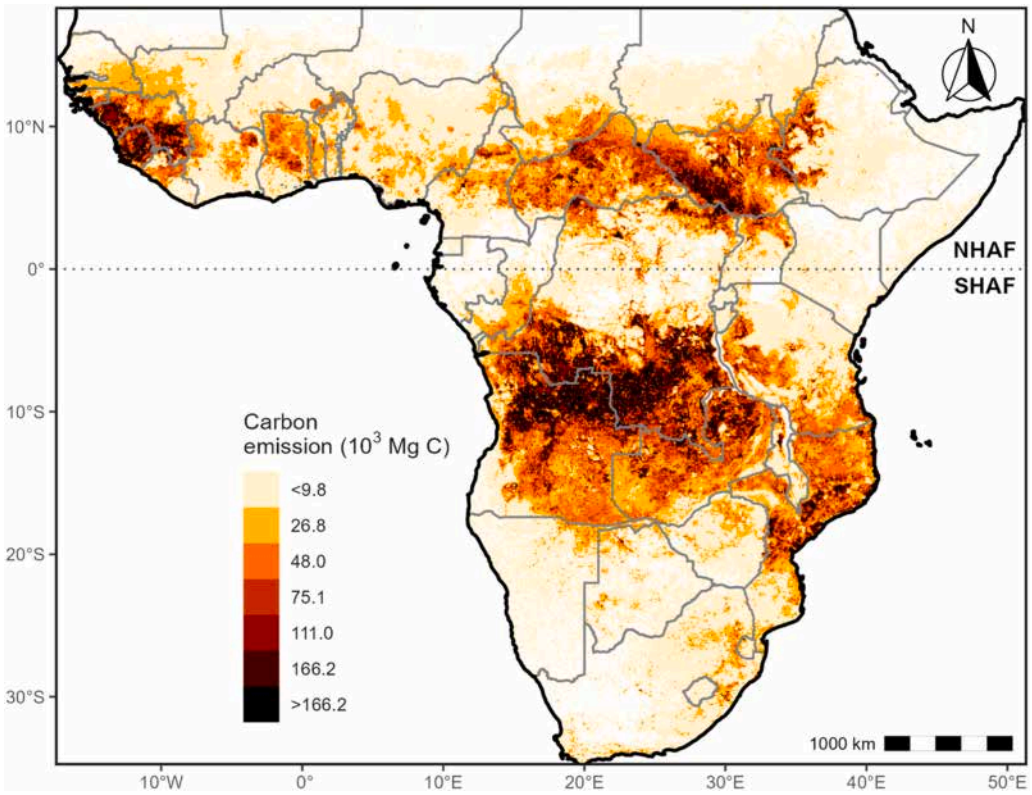

Fig. 4. Spatial distribution of fire carbon emissions using VIIRS-EM for 2013–2022 across sub-Saharan Africa. VIIRS-EM, highlighting two major fire belts—the northern tropical savannas (~5–15°N) and the southern dry woodlands (~5–15°S). Units: 1 Pg C = 1 000 Tg C = 10^6 Gg C = 10^9 Mg C = 10^9 t C.

continuous fuels.

4.3. Seasonal dynamics and contribution of small fires

Incorporating small fires not only increases total emissions but also alters the seasonal pattern of fire activity across SSA. Fire regimes in the region are strongly influenced by rainfall seasonality: Northern Hemisphere savannas typically burn between November and February (dry season), while Southern Hemisphere ecosystems experience peak fire activity between May and September. Coarse-resolution satellite data often depict a shortened fire season concentrated near the driest months, primarily capturing large, intense fires. In contrast, our high-resolution VIIRS-EM inventory reveals a more extended and temporally distributed pattern, with significant emissions during the early and late stages of the fire season. These periods tend to be dominated by smaller, short-lived burns that are underrepresented in coarse-resolution datasets.

Fig. 5 shows the monthly distribution of carbon emissions for NHAF and SHAF, comparing VIIRS-EM with MODIS-EM. In NHAF, VIIRS-EM emissions exceed those of MODIS-EM particularly during the early fire season (October–November) and again toward the end (March–April). During the mid-season peak (December–January), the two estimates converge more closely. In June, VIIRS-EM emissions are over 80 % higher than MODIS-EM, and in months such as July and August, differences exceed 140 %. These are periods when smaller fires may dominate but are poorly captured by MODIS. An exception occurs in December in NHAF, where MODIS-EM slightly exceeds VIIRS-EM by approximately 3 %. This may be due to differences in pre-processing: VIIRS-EM excludes all low-confidence detections (i.e., those not classified as "nominal" or "high" in the VNP14IMG product), whereas MODIS-EM retains fires with confidence above 50 %. During transitional months like December, some lower-intensity fires may be filtered out by VIIRS while still passing the MODIS threshold, resulting in a rare month where MODIS detects slightly more fire activity.

In SHAF, the seasonal differences are especially pronounced at the onset of the fire season (February–April). In these early months, VIIRS-EM emissions exceed MODIS-EM by up to 69 %, reflecting the improved ability of VIIRS to detect low-intensity fires at the beginning of the dry season. During the peak fire months (July–August), both sensors detect a large number of fires, and their estimates converge more closely, although VIIRS-EM continues to report slightly higher emissions overall. The inclusion of small fires captured by VIIRS thus extends the effective fire season, adding a substantial volume of emissions during the months that precede and follow the main burning period.

A similar seasonal enhancement is observed when comparing the FINN inventories. FINN_viirs consistently reports 20–40 % higher emissions than FINN_modis across most months in both hemispheres. This difference highlights the effect of increased fire detection frequency, including additional nighttime and low-FRP events, even within a shared modelling framework.

This seasonal extension is particularly relevant for regional greenhouse gas inventories, as it indicates that conventional approaches likely underestimate fire emissions not only in magnitude but also in terms of combustion timing and seasonality. In Southern Africa, for example, VIIRS-EM detects considerable fire activity during April and May, prior to the main fire peak in July–September. This pattern suggests that the duration of the active fire season is longer than typically represented in existing emission inventories.

4.4. Inventory biases and discrepancies

To evaluate discrepancies across fire emission inventories, we analysed the spatial distribution of relative bias between our VIIRS-EM small fire dataset (defined as FRP $<$ 10 MW) and six widely used global fire products. The results are presented in Fig. 5, which highlights the relative differences at the pixel scale across SSA. These maps focus specifically on small fires, while full-inventory comparisons based on all

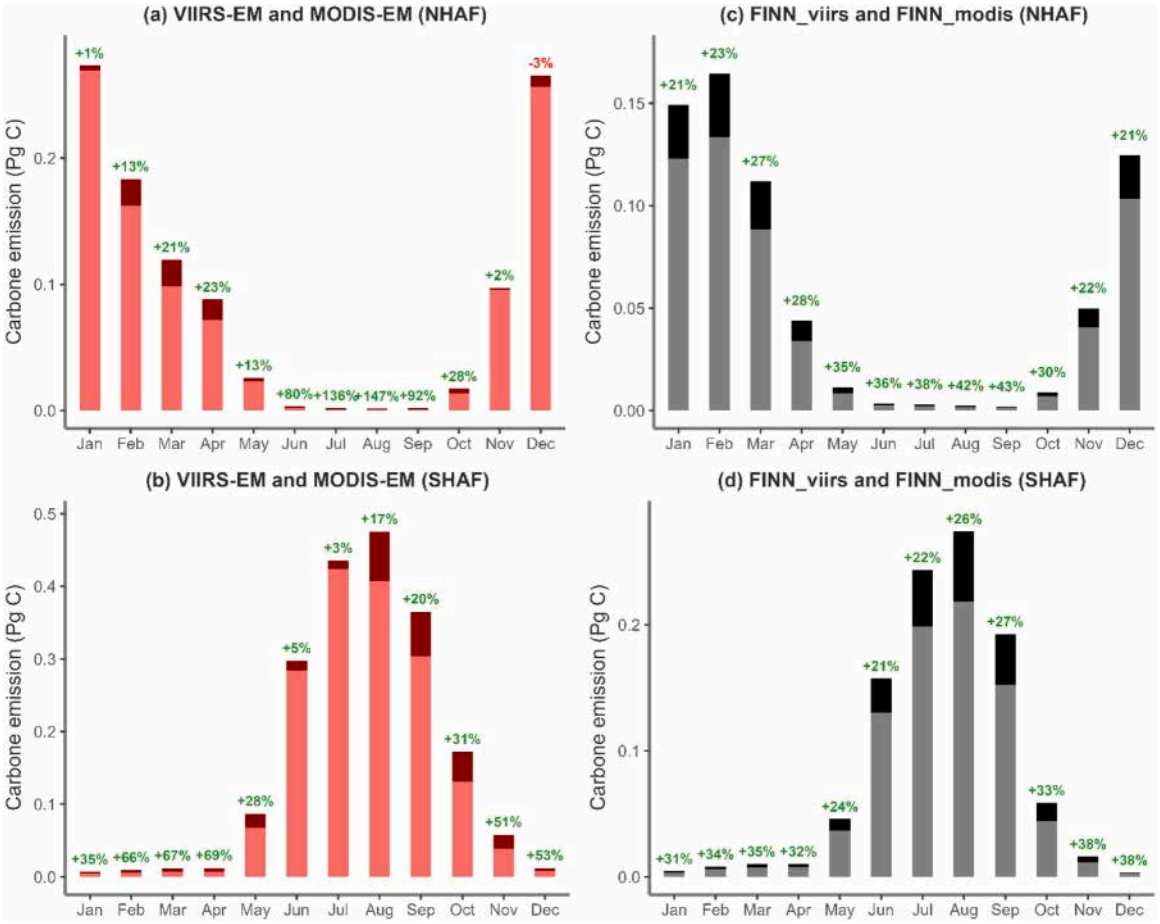

Fig. 5. Monthly fire carbon emissions and relative differences across NHAF and SHAF regions (average 2013–2022). (a–b) Comparison of monthly carbon emissions from VIIRS-EM and MODIS-EM in NHAF (a) and SHAF (b). Bars show MODIS-EM (base) with VIIRS-EM stacked above, and percentage labels indicate relative difference. (c–d) Same comparison for FINN_viirs and FINN_modis. Small fires detected by VIIRS add significantly to emissions during early and late fire-season months. December anomalies in NHAF may reflect detection filtering thresholds. Units: 1 Pg C = 1 000 Tg C = 10^6 Gg C = 10^9 Mg C = 10^9 t C.

VIIRS-EM emissions are provided separately in Appendix Figure A1.

MODIS-era inventories consistently report lower emissions in regions dominated by low-FRP fires (Fig. 6), with mean biases ranging from −76 % to −34 %.

- FINN_modis shows the strongest underestimation, with a mean relative bias of −76.3 % and limited variability (standard deviation: 27.4 %). Near-maximum underestimation (−100 %) is observed across extensive zones. This reflects MODIS's limited capacity to

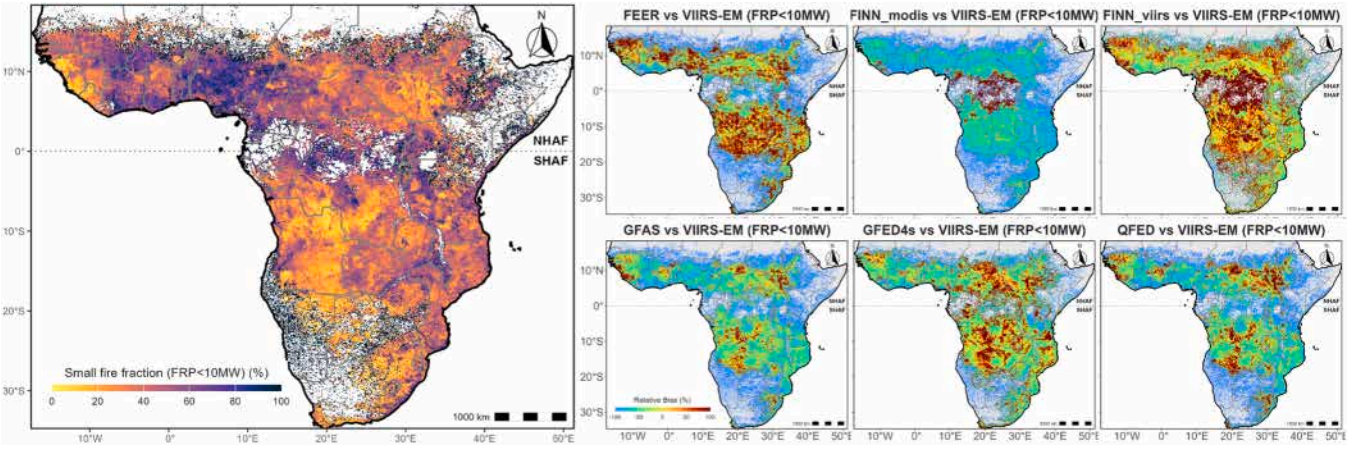

Fig. 6. Relative bias (%) of six global fire emission inventories compared to VIIRS-EM (small fires only, FRP < 10 MW), across sub-Saharan Africa for the period 2013–2022. (right panel) Blue areas indicate where the inventory reports lower emissions than VIIRS-EM; red areas show higher estimates. Clear underestimation patterns are observed in key fire regions, particularly in West, Central, and Southern Africa. MODIS-based inventories (GFED4s, GFAS, QFED, FEER, FINN_modis) show widespread negative biases, while FINN_viirs— which includes VIIRS detections—shows better agreement with the VIIRS-EM reference. For comparison with the full VIIRS-EM dataset (not limited to small fires), see Appendix Figure A1. Units: 1 Pg C = 1 000 Tg C = 10^6 Gg C = 10^9 Mg C = 10^9 t C.

detect small, low-intensity fires, especially in fragmented land mosaics.

- GFAS exhibits a similarly high negative bias (mean: −57.7 %; standard deviation: 45.7 %), with strong underestimation in fire-active regions such as West Africa (Senegal, Mali, northern Côte d'Ivoire; approx. 10–15° N, 5–15° W), Central Africa (southern Chad, northern Central African Republic, northern DRC; approx. 5–10° N, 15–30° E), and Southern Africa (Angola, northern Mozambique, eastern Zambia; approx. 10–20° S, 15–35° E).
- QFED shows similarly widespread underestimation, with relative biases in the range of −60 % to −80 % across large areas. Despite being tuned to match aerosol optical depth (AOD) observations, QFED remains limited by its reliance on MODIS FRP, which constrains its ability to represent fine-scale and low-intensity burning.
- FEER and GFED4s present more moderate mean biases of −38.9 % and −33.7 %, respectively, but with high dispersion (standard deviations > 50 %). Although GFED4s includes a small-fire correction, it does not fully resolve local fire variability. FEER occasionally exceeds VIIRS-EM in regions with dense smoke (northern Angola), likely due to emission coefficients tuned using satellite-derived aerosol optical depth.
- In contrast, FINN_viirs, which includes VIIRS fire detections, aligns more closely with the small-fire VIIRS-EM reference. Its mean bias is only −9.1 %, and the majority of grid cells fall within ±25 % deviation. Spatial patterns in FINN_viirs are more consistent with VIIRS-EM, highlighting the benefits of using high-resolution fire detection inputs.

These results demonstrate a systematic contrast between MODIS-based and VIIRS-based inventories. Products relying solely on MODIS data significantly underestimate emissions in regions with high densities of small fires, while VIIRS-based inventories (or those incorporating VIIRS data) offer better consistency with independent small-fire estimates. This distinction is particularly important in the savanna-agriculture transition zones of West, Central, and Southern Africa, where fire fragmentation is common and underdetection is widespread.

To explore whether the small-fire fraction alone explains these discrepancies, we conducted a binned scatter analysis (Figure A2, Appendix). The relationship between the relative bias and the proportion of FRP from small fires (FRP < 10 MW) is weak for all inventories, with coefficients of determination (R^2) below 0.15. This suggests that while small fires contribute to underestimation, other factors such as region-specific combustion characteristics, fuel availability, and fire detection methodology also play a role.

5. Discussion

5.1. Magnitude gap between VIIRS-EM and legacy inventories

The higher total emissions reported by VIIRS-EM compared to other global fire emission inventories can be attributed to several complementary factors, primarily related to fire detection capability, land use context, and methodological design. Although the technical differences between sensors are well established, the magnitude of the divergence observed in this study, often exceeding 50–75 % in annual totals, warrants closer examination of the underlying causes.

One of the key factors is the improved detection of small, fragmented fires by VIIRS. Coarse-resolution sensors such as MODIS tend to miss short-duration or low-intensity fires, particularly those occurring in heterogeneous landscapes. These include savanna–cropland mosaics in West and Central Africa, where field-clearing or residue-burning practices generate small but frequent fires that are below MODIS detection thresholds. As demonstrated in FireCCISFD20-based BA estimates [51], these fires can account for a substantial share of total fire activity in agricultural zones but are not represented in inventories relying on moderate-resolution BA mapping.

The spatial distribution of fire emissions observed in VIIRS-EM aligns with patterns identified in recent satellite-based atmospheric studies. Multiple research efforts have demonstrated the influence of biomass burning on trace gas concentrations, especially carbon monoxide (CO), as captured by instruments such as TROPOMI, MOPITT, and VIIRS. For instance, Griffin et al. [25] showed that FRP can be directly linked to CO column enhancements detected by TROPOMI, with regional differences reflecting vegetation type and fire regime. Similarly, [41] validated MOPITT CO retrievals using in situ AirCore profiles, highlighting how satellite observations capture tropospheric CO variability during active fire seasons.

In our study, VIIRS-EM emission hotspots often coincide with regions exhibiting high aerosol optical depth and elevated CO concentrations reported in prior literature. This spatial consistency supports the interpretation that coarse-resolution inventories may underestimate fire emissions in key fire-prone areas, particularly in agricultural and savanna mosaics. Recent multi-platform experiments such as FIREX-AQ [57] and global assessments by Kloss et al. [32] further confirm that large-scale fire activity contributes significantly to atmospheric trace gas loading and can lead to long-range pollutant transport.

Although our analysis does not directly assimilate satellite-based trace gas retrievals, the consistency between VIIRS-EM spatial patterns and satellite-observed atmospheric enhancements strengthens the case for using high-resolution fire emission datasets in air quality and climate modelling. This approach is also in line with recent calls to integrate observational data with emission modelling to better constrain fire-related impacts on atmospheric composition [13].

This spatial consistency supports the interpretation that coarse-resolution inventories may underestimate fire emissions in key fire-prone areas, particularly in agricultural and savanna mosaics. This is in line with findings by Garrigues et al. [19], who showed that BA–based products often fail to reproduce satellite-observed atmospheric pollutant loads over fragmented land-use regions. The limitations of MODIS FRP are also well documented. Studies such as Li et al. [37] demonstrated that MODIS underdetects low-FRP fires in Africa by a wide margin compared to VIIRS. This helps explain why FRP-assimilated products like GFAS or FRP-tuned inventories such as QFED continue to report significantly lower emissions, even in regions with high fire activity.

In parallel, declining BA trends in Africa over the last decade may partially obscure ongoing fire activity in inventory time series that rely solely on area-based metrics. This decline has been documented by several satellite-based studies [38,64,2] and is likely influenced by land use transitions, including agricultural expansion, intensification of land management, and the implementation of fire suppression policies. These processes reduce fuel continuity and limit the spread of large fires, particularly in savanna and agro-ecological regions where extensive burning was historically common [48,54].

In this context, an FRP-based approach like VIIRS-EM captures combustion events that are otherwise missed due to both resolution and conceptual limitations. By integrating satellite observations with land cover–specific combustion characteristics, VIIRS-EM provides a more temporally and spatially complete representation of fire emissions in SSA. This improves not only total emission quantification but also the spatial realism of inputs used in air quality and climate models.

5.2. Linking emission biases to biogeochemical and atmospheric consequences

5.2.1. Global greenhouse gas budgets

African fires represent a significant component of the global carbon cycle, yet they remain systematically underestimated in many current inventories. Our findings confirm that the omission of small fires and low-intensity burns in coarse-resolution satellite products has led to substantial underreporting of fire emissions in sub-Saharan Africa, with differences reaching 50–75 % in some datasets. While the immediate effect is a higher regional carbon total (3.0 Pg C yr^{-1} in our VIIRS-EM

estimate), the broader implication is that global carbon cycle assessments relying on MODIS-era products likely miss a considerable portion of biospheric carbon fluxes.

Although much of the CO_2 emitted from fire is considered "biogenic" and assumed to be re-sequestered through post-fire regrowth, the magnitude of African fire emissions (approximately 11 000 Tg CO_2 yr^{-1}) suggests that any persistent bias can distort the baseline for land–atmosphere carbon exchange. In regions where savannas and woodlands are undergoing land-use change, this uncertainty becomes more consequential. Fire also interacts with vegetation recovery, and the reabsorption of carbon is neither immediate nor complete [45]. By refining estimates of the initial release phase, our inventory contributes to more accurate net ecosystem exchange calculations and reduces potential bias in climate feedback assessments.

Including small fires in emissions accounting improves regional estimates and contributes to narrowing gaps in global CO_2 budgets. Coarse-resolution inventories often miss diffuse agricultural burning and low-intensity fires, which are especially relevant in African landscapes. As fire emissions are increasingly used to constrain atmospheric inversion models and inform national greenhouse gas inventories, high-resolution products such as VIIRS-EM provide meaningful improvements. These enhancements are particularly relevant to global assessments led by initiatives such as the Global Carbon Project and to national reporting under the Paris Agreement, as reflected in the IPCC Sixth Assessment Report [18,29] .

5.2.2. Ecological feedbacks

Small fires also have ecological relevance. In savanna and agro-pastoral systems across sub-Saharan Africa, small fires, often ignited for land management, generate a mosaic burn pattern [34]. This patchwork reduces fuel continuity and may lower the probability or intensity of subsequent large wildfires [5]. Their omission from traditional fire inventories affects not only total emissions but also the representation of fire–vegetation interactions in models. Earth system models that simulate vegetation dynamics and fire behaviour, such as those participating in the Fire Modeling Intercomparison Project (FireMIP; [47]), often operate at spatial resolutions too coarse to resolve small, patchy burns. This can result in overestimated fuel accumulation and delayed peak fire intensity if frequent early-season fires are not accounted for.

High-resolution satellite observations, such as those used in this study, indicate that although small fires increase cumulative carbon emissions, they also influence fire regime characteristics, including timing, recurrence, and combustion conditions. These fires tend to be more smouldering than flaming [14,61], which affects the CH_4 to CO_2 emission ratio and alters the vertical structure of smoke plumes.

Further development of fire models could integrate FRP-based approaches like VIIRS-EM into dynamic fire–vegetation models to benchmark more realistic fire size distributions [26], and better simulate trace gas partitioning, and feedback mechanisms. Such integration would improve emission estimates while enhancing the ecological realism of fire simulations in African landscapes. In addition to influencing vegetation structure, repeated small fires may also affect regional climate by altering surface albedo and evapotranspiration [63], particularly in savanna–forest transition zones. These feedbacks are not well represented in current coupled land–atmosphere models and merit further investigation.

5.2.3. Atmospheric chemistry and air quality

The accuracy of fire emission inventories directly affects the performance of atmospheric composition models. Our results indicate persistent underestimation of emissions across Africa. These biases can result in underprediction of pollutant concentrations in both regional and global chemical transport models. The VIIRS-EM inventory addresses this issue by capturing early-season agricultural fires and spatially dispersed small burns that are dominant sources of CO and CH_4 but often remain undetected by MODIS-based datasets.

Improved representation of small fires enhances satellite data assimilation and model–observation consistency. Recent studies, including van der Velde et al. [55], have shown that using high-resolution BA data, such as Sentinel-2 at 20 m, can increase estimated fire emissions by up to 120 % in southern Africa. This adjustment leads to better alignment with satellite-based CO observations, particularly those from TROPOMI, and reduces the bias in modelled CO columns by around 15 %. The FRP-based method used in this study, which does not rely on explicit BA mapping, achieves similar improvements. Its higher sensitivity allows it to capture fire activity that is often omitted in lower-resolution datasets.

Improved seasonal representation in VIIRS-EM, including emissions from the early and late dry season, also enhances the simulation of secondary pollutants. For example, ozone formation depends on the timing and spatial overlap of NO_x and VOC emissions with sunlight exposure. If emissions are too narrowly distributed in time, models may misrepresent the chemical environment and underestimate surface ozone levels.

Aerosol-related effects are also substantial. Biomass burning in SSA contributes significantly to black carbon and organic aerosol loading, affecting visibility, radiative forcing, and cloud formation (X. [39]). Despite this, many atmospheric models underpredict aerosol optical depth during the fire season. VIIRS-EM, with its higher emission estimates and improved spatial and temporal resolution, may help reconcile model outputs with satellite-based AOD retrievals, especially in regions heavily influenced by fire plumes such as Angola, Zambia, and the central Congo basin. Vertical injection height of emissions, which varies with fire intensity and atmospheric stability, also influences the long-range transport of pollutants [24]. African fire plumes can reach the free troposphere, facilitating intercontinental transport to the Atlantic and South America. Improved quantification of injection profiles remains a gap in current models. Multi-sensor validation using instruments such as MOPITT (for CO), IASI (for NH_3), and CALIPSO (for aerosol vertical profiles) could provide additional constraints on fire plume characteristics. These observations would help validate model performance across trace gases and altitudes, particularly in regions where ground-based data are sparse.

The improved spatial and temporal fidelity of VIIRS-EM has direct implications for air quality forecasting, climate model aerosol forcing assessments, and satellite product validation. It provides a valuable step toward resolving persistent mismatches between modelled and observed trace gases and aerosols in one of the most fire-affected regions globally.

5.3. Toward improved climate reporting and policy

Accurate fire emission inventories are essential not only for advancing scientific understanding but also for supporting climate policy, mitigation planning, and air quality governance. While the IPCC provides methodological guidance for distinguishing anthropogenic from natural fire emissions, final classification is determined at the national level. In savanna-dominated regions such as sub-Saharan Africa, this distinction is often unclear, since many fires are intentionally set for agricultural or pastoral use but occur in ecosystems categorized as "natural" under some reporting protocols. Our results indicate that reliance on coarse-resolution MODIS-based products may contribute to systematic underestimation of fire emissions in both scientific evaluations and policy frameworks.

Although most countries do not yet report fire emissions separately, in part due to difficulties in tracking vegetation regrowth and assigning anthropogenic attribution, the growing integration of satellite-based inventories into global assessment systems and nationally determined contributions (NDCs) makes it increasingly important to address these uncertainties [42].

As climate transparency mechanisms such as the Global Stocktake [46], the Global Methane Pledge [23], and regional air quality

agreements evolve, the demand for spatially detailed and temporally consistent emission data continues to increase. Inventories such as GFED4s and GFAS, which omit large numbers of small and early-season fires, may be insufficient for informing mitigation strategies in countries where fire plays a central role in land use and ecosystem dynamics.

Our VIIRS-EM inventory helps address these gaps by providing emissions data with improved spatial resolution and seasonal structure. This enhances total carbon accounting and strengthens the capacity to track short-lived climate forcers such as methane and aerosols with greater accuracy. The inventory aligns with the goals of emerging climate-monitoring frameworks, which emphasize completeness, consistency, and transparency of emissions data.

Improved inventories also have value for co-benefits analysis. For example, more accurate estimates of fire-related methane and $PM_{2.5}$ can inform assessments of public health risks, support early warning systems for smoke exposure, and guide policies that integrate land management with air quality objectives [31]. Countries experiencing agricultural expansion or land-use transitions may benefit from updated, high-frequency emission datasets such as those generated using VIIRS. These data enable monitoring at subnational scales with greater temporal and spatial granularity than earlier-generation products.

Fire emissions influence several components of the Earth system, including atmospheric composition, surface radiation balance, vegetation dynamics, and precipitation regimes. In sub-Saharan Africa, smoke aerosols contribute to cloud modification, while trace gases such as carbon dioxide and ozone precursors affect both air quality and regional climate forcing. These interactions can create feedbacks that reinforce fire activity under certain environmental conditions.

By capturing a broader spectrum of fire activity, particularly small and early-season events, VIIRS-based products help reduce long-standing biases in regional carbon budgets. This is especially valuable for improving the accuracy of Earth system models and atmospheric inversion systems. Nonetheless, the relatively short duration of the VIIRS record limits its use for long-term climate trend analysis. A promising path forward is to calibrate or bias-correct MODIS-based FRP observations using the VIIRS overlap period, thereby extending high-resolution emission estimates further back in time while maintaining methodological consistency.

5.4. Uncertainties and further improvements

Although the VIIRS-EM inventory offers a refined and physically consistent estimate of fire emissions across SSA, several sources of uncertainty remain. Despite its improved spatial resolution and sensitivity compared to MODIS, the VIIRS sensor is still subject to detection limitations. Fires obscured by persistent cloud cover, burns beneath dense forest canopies, or very short-duration events may not be observed. To reduce these effects, the analysis excluded low-confidence fire detections and focused on fire signals persistent over multiple days. Nevertheless, undetected events may still occur, particularly in humid or densely vegetated regions where observational challenges remain even for high-resolution sensors. The inventory may also miss some fire activity captured by other methodologies such as FINN_viirs, which infers BA through clustering of active fire detections. These differences highlight the importance of both sensor sensitivity and methodological design in shaping total emissions. Recent work on active fire clustering and spatiotemporal dynamic modelling demonstrates the potential to enhance fire delineation for more accurate emissions estimation [11].

In addition, uncertainties persist in the conversion from FRP to biomass consumption. This study improved upon the common assumption of a fixed FRP-to-biomass ratio by applying land cover–specific coefficients, following Akagi et al. [1]. However, these coefficients are based on average combustion characteristics and may not fully reflect variability in fuel moisture, fire intensity, or landscape conditions. For instance, savanna fires in western and southern Africa may differ in combustion efficiency due to rainfall gradients or land use intensity, yet are assigned a uniform coefficient. Regional calibration or seasonally adjusted values could improve this aspect, particularly if supported by field measurements or inversion-based constraints. Despite these limitations, the approach used here represents a significant step toward reducing bias introduced by oversimplified combustion assumptions. Future versions of this inventory could take advantage of the VIIRS Active Fires Collection 2 [20], which not only improves detection sensitivity and reduces commission errors but also combines observations from both Suomi-NPP and NOAA-20. The joint use of the two VIIRS platforms is expected to enhance temporal coverage and consistency, thereby providing a stronger observational basis for fire emissions estimates.

EFs are another source of uncertainty. This analysis used mean values per species and biome from Andreae [3], and where available, included ± 1 standard deviation to represent within-biome variability. Trace gas yields can vary substantially depending on fire phase, fuel type, and combustion conditions. For species such as CH_4 and CO, variability in EFs is especially pronounced. Fires occurring earlier in the dry season tend to be more smouldering and release relatively more CH_4, whereas late-season fires are typically more flaming and produce proportionally more CO_2 [61]. Capturing this full combustion spectrum may require temporally resolved EFs. Ongoing field campaigns such as SAFARI and AFCAM are expected to provide new data to refine African-specific EFs. Machine learning techniques for dynamic EF adjustment [56] may also offer a path forward to reduce this source of uncertainty.

Another source of uncertainty is the classification of land cover types used to assign combustion coefficients and LULC. The MODIS MCD12Q1 product is subject to misclassification, particularly in ecotonal regions and agricultural mosaics. Errors in land cover assignment may affect the selection of biome-specific parameters and introduce spatially variable bias, especially where fire dynamics differ between natural vegetation and human-managed landscapes.

The threshold used to identify small fires (FRP < 10 MW) also introduces potential ambiguity. It is important to note that our definition of small fires is based on FRP, not BA, although low-FRP events often coincide with relatively small or short-lived burns. This value is based on the approximate detection limits of MODIS, and serves as a proxy for low-intensity and sub-resolution burns. However, some low-FRP detections may originate from the smouldering edges of larger fires, and conversely, some small but intense fires could exceed the threshold briefly. Future work could explore context-specific or adaptive thresholds to better isolate fine-scale fire activity, potentially improving attribution of emission discrepancies in fragmented landscapes.

Direct validation of the VIIRS-EM inventory was not performed in this study, which we recognize as a limitation. While our analysis demonstrates internal consistency and aligns with expected fire patterns, a rigorous evaluation against independent data remains an important next step. Validation with atmospheric observations remains an area for future improvement. Although this study did not directly compare emissions with satellite-derived CO columns (from TROPOMI or GOSAT), prior work has shown that including small fires enhances consistency with such data. For example, van der Velde et al. [55] found that adding small fires improved agreement between fire inventories and observed CO concentrations over Southern Africa. Future efforts could build on this by assessing whether spatial and seasonal emissions patterns align with trace gas retrievals, and by using such data to inform adjustments to FRP-to-biomass ratios or EF estimates in a constrained modelling framework.

Finally, although the VIIRS-EM approach is designed to be scalable, applying it outside SSA will require adjustments for local fire regimes, land cover distributions, and detection environments. As such, while the framework provides a valuable foundation for broader application, regional calibration will be essential to ensure reliability and accuracy in other parts of the world. It is important to emphasize that in this study, fire typologies were primarily used to assign land-cover–specific

combustion coefficients and EF, thereby ensuring biome-specific representativeness in global emission estimates. A detailed analysis of emissions by vegetation type lies beyond the scope of this paper but is the focus of ongoing work. Typologies are therefore revisited here only to situate the results within broader agro-climatic contexts rather than as explicit result categories.

6. Conclusion

This study presents a high-resolution fire emission inventory for SSA based on active fire detections from the VIIRS sensor and a top-down approach using FRP. The method enables the estimation of carbon emissions at 0.1° spatial resolution using consistent processing of satellite data, land cover classification, and biome-specific emission parameters. The resulting VIIRS-based emission dataset (VIIRS-EM) was evaluated alongside a MODIS-based counterpart (MODIS-EM) and six widely used global fire inventories.

Compared to existing MODIS-era products, VIIRS-EM yields significantly higher emission estimates across SSA, with average annual fire carbon emissions of 3.0 Pg C. These differences are primarily attributed to the improved detection of small, low-intensity fires by VIIRS. Such fires are common in agricultural and savanna landscapes and are typically underrepresented in coarser-resolution BA products. Our results demonstrate that current global inventories systematically underestimate emissions by 50–75 % in many areas, particularly in regions with fragmented fire regimes. The additional MODIS-EM product confirms that sensor resolution and detection capability account for a large portion of these differences.

We further isolated and evaluated emissions from small fires using a threshold of FRP < 10 MW. These small fires contribute significantly to early and late dry-season emissions and explain much of the seasonal underrepresentation observed in existing inventories. By quantifying the contribution of small fires and comparing them with other datasets, our approach highlights the structural limitations of conventional inventories in capturing the full spectrum of fire activity in SSA.

The VIIRS-EM dataset provides enhanced spatial and temporal coverage of fire emissions, offering improvements in both carbon accounting and atmospheric modelling inputs. This refinement is particularly valuable for air quality forecasting, satellite data assimilation, and the assessment of short-lived climate forcers. It also supports improved reporting and transparency under frameworks such as the Paris Agreement.

Nonetheless, several sources of uncertainty remain. These include sensor detection limits under cloudy conditions, variability in combustion efficiency across landscapes, and static EFs. While the current product focuses on carbon dioxide, the methodology can be extended to other species if adequate EFs are available. Future work should prioritize validation with atmospheric observations and explore opportunities to calibrate MODIS-era fire records using the VIIRS time series.

In conclusion, our findings reinforce the importance of high-resolution satellite data and FRP-based methods in improving the quantification of fire emissions in Africa. The VIIRS-EM inventory prototype represents a meaningful step toward reducing uncertainties in the regional fire carbon budget and contributes to more accurate integration of African fire dynamics in global climate assessments.

CRediT authorship contribution statement

Barbara Sponholz: Writing – review & editing, Supervision, Funding acquisition. **Frédéric Chevallier:** Writing – review & editing, Writing – original draft, Methodology, Data curation. **Florent Mouillot:** Writing – review & editing, Writing – original draft, Validation, Methodology, Data curation, Conceptualization. **Michael Thiel:** Writing – review & editing, Writing – original draft, Validation, Supervision, Funding acquisition, Data curation, Conceptualization. **Boris Ouattara:** Writing – review & editing, Writing – original draft, Methodology, Formal analysis, Data curation, Conceptualization.

Declaration of Competing Interest

The authors declare the following financial interests/personal relationships which may be considered as potential competing interests: Boris Ouattara reports financial support was provided by German Federal Ministry for Education and Research (BMBF). If there are other authors, they declare that they have no known competing financial interests or personal relationships that could have appeared to influence the work reported in this paper.

Acknowledgements

The authors acknowledge the support from the German Federal Ministry for Education and Research (BMBF) via the project carrier at the German Aerospace Center (DLR Projektträger) through the research projects: WASCAL-DE-Coop (FKZ: 01LG1808A) and NetCDA (FKZ: 01LG2301A). We also express our sincere gratitude to the research teams and institutions that have developed and maintained the global fire emission inventories utilized in this study. Their foundational work has been instrumental in advancing our understanding of biomass burning emissions and continues to serve as a cornerstone for ongoing scientific research. Specifically, we acknowledge:

- Global Fire Emissions Database (GFED4s): Developed by the team led by Randerson et al., providing comprehensive data on burned area and fire emissions.
- Global Fire Assimilation System (GFAS): Produced by the Copernicus Atmosphere Monitoring Service (CAMS) at ECMWF, offering daily estimates of biomass burning emissions based on satellite observations.
- Quick Fire Emissions Dataset (QFED): Developed by the NASA Goddard Space Flight Center, delivering near-real-time emissions data derived from satellite fire observations.
- Fire Energetics and Emissions Research (FEER): Created by Ichoku and Ellison, providing emissions estimates based on fire radiative energy measurements.
- Fire INventory from NCAR (FINN): Developed by the National Center for Atmospheric Research (NCAR), offering high-resolution, global estimates of trace gas and particle emissions from open burning.

Their contributions have been invaluable in facilitating comparative analyses and enhancing the accuracy of fire emission assessments in our research.

Appendix

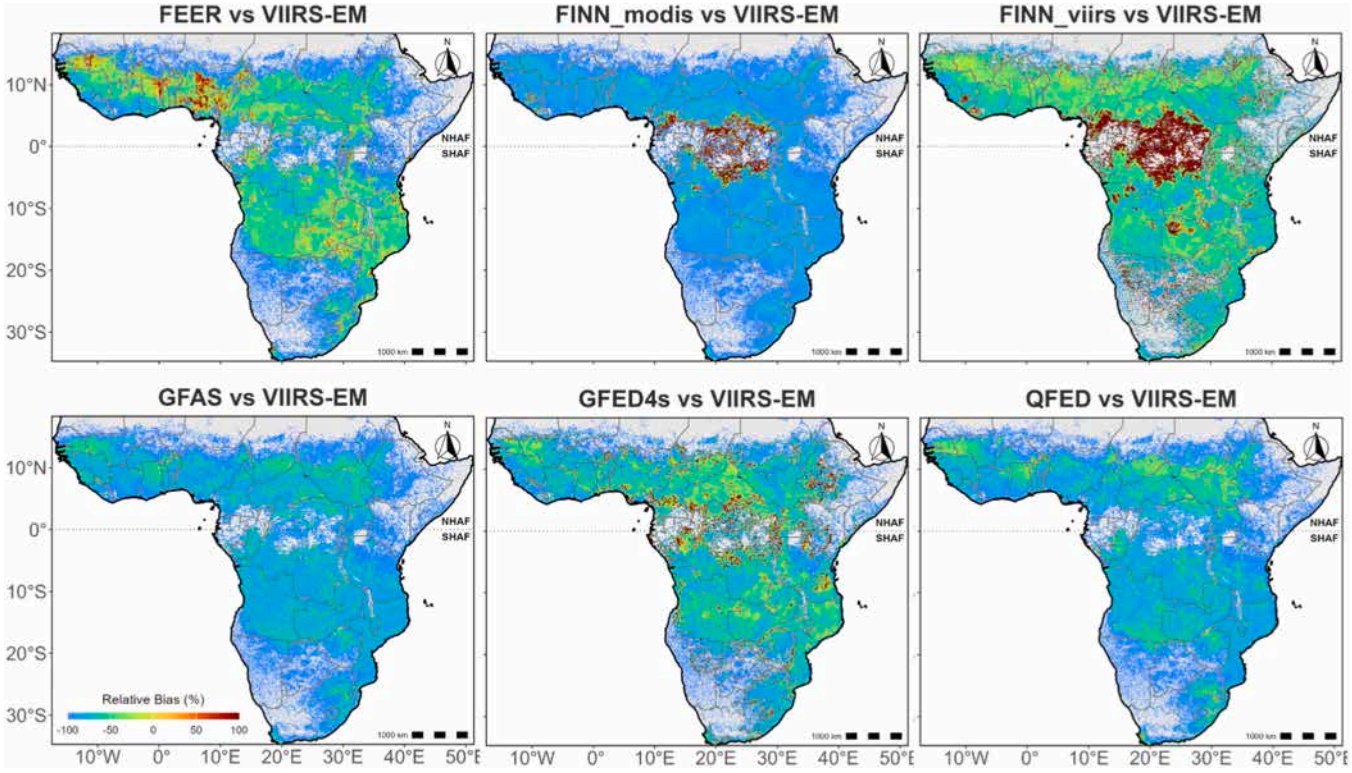

Fig. A1. Relative bias (%) of six global fire emission inventories compared to the full VIIRS-EM dataset (all fires), averaged over 2013–2022. Unlike Fig. 5, this comparison includes both large and small fires. Blue areas indicate underestimation relative to VIIRS-EM; red indicates overestimation. While small fire-dominated regions show strong bias, some inventories (e.g., FEER) show local overestimation in regions with frequent dense smoke, possibly due to AOD-based tuning. Units: 1 Pg C = 1 000 Tg C = 10^6 Gg C = 10^9 Mg C = 10^9 t C

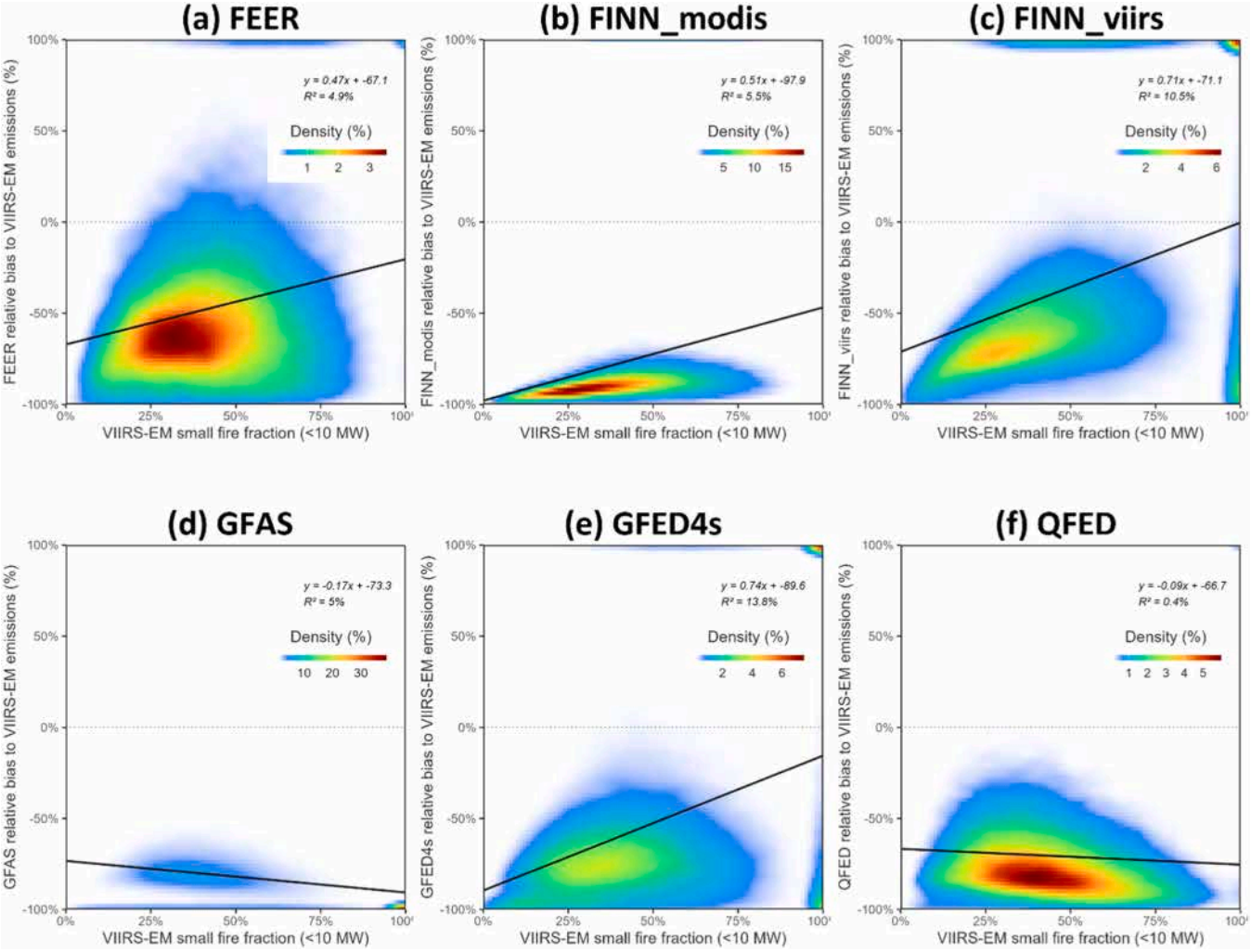

Fig A2. Scatterplots of relative bias (%) in carbon emissions versus small fire fraction (FRP < 10 MW) across SSA grid cells, for six global fire inventories compared to VIIRS-EM. Each panel displays binned point density (color scale) and the linear regression fit (black line). All relationships are weak, with R^2 ranging from 0.4 % to 13.8 %. This indicates that while small fire prevalence is a relevant explanatory variable, it alone does not account for the full magnitude of inventory bias. Density values represent the relative abundance of grid cells in each bin

Data availability

Data will be made available on request.

References

[1] S.K. Akagi, R.J. Yokelson, C. Wiedinmyer, M.J. Alvarado, J.S. Reid, T. Karl, J. D. Crounse, P.O. Wennberg, Emission factors for open and domestic biomass burning for use in atmospheric models, Atmos. Chem. Phys. 11 (9) (2011) 4039–4072, https://doi.org/10.5194/acp-11-4039-2011.

[2] N. Andela, D.C Morton, L. Giglio, Y. Chen, G.R van der Werf, P.S Kasibhatla, R. S DeFries, G.J Collatz, S. Hantson, S. Kloster, D. Bachelet, M. Forrest, G. Lasslop, F. Li, S. Mangeon, J.R Melton, C. Yue, J.T Randerson, A human-driven decline in global burned area, Science (2017), https://doi.org/10.1126/science.aal4108.

[3] M.O. Andreae, Emission of trace gases and aerosols from biomass burning – an updated assessment, Atmos. Chem. Phys. Discuss. (2019) 1–27, https://doi.org/10.5194/acp-2019-303.

[4] S. Archibald, D.P. Roy, B.W. van Wilgen, R.J. Scholes, What limits fire? An examination of drivers of burnt area in Southern Africa, Glob. Change Biol. (2009), https://doi.org/10.1111/j.1365-2486.2008.01754.x.

[5] S. Archibald, A.C. Staver, S.A. Levin, Evolution of human-driven fire regimes in Africa, Proc. Natl. Acad. Sci. (2011), https://doi.org/10.1073/pnas.1118648109.

[6] S.E. Bauer, U. Im, K. Mezuman, C.Y. Gao, Desert dust, industrialization, and agricultural fires: health impacts of outdoor air pollution in Africa, J. Geophys. Res. Atmospheres (2019), https://doi.org/10.1029/2018jd029336.

[7] M.H. Bhuian, H. Dastour, M.R. Ahmed, Q.K. Hassan, Comparison of perimeter delineation methods for remote sensing fire spot data in near/ultra-real-time applications, Fire 7 (7) (2024) 226, https://doi.org/10.3390/fire7070226.

[8] E. Chuvieco, F. Mouillot, G.R. van der Werf, J. San Miguel, M. Tanasse, N. Koutsias, M. García, M. Yebra, M. Padilla, I. Gitas, A. Heil, T.J. Hawbaker, L. Giglio, Historical background and current developments for mapping burned area from satellite earth observation, Remote Sens. Environ. 225 (March) (2019) 45–64, https://doi.org/10.1016/j.rse.2019.02.013.

[9] Copernicus Emergency Management Service. (2024). Active Fire Detection - Technical Background. ⟨https://forest-fire.emergency.copernicus.eu/about-effis/technical-background/active-fire-detection⟩.

[10] Darmenov, A.S., & Silva, A. (2015). The Quick Fire Emissions Dataset (QFED): Documentation of versions 2.1, 2.2 and 2.4, NASA Technical Report Series on Global Modeling and Data Assimilation, NASA/TM-2015-104606. Technical Report Series on Global Modeling and Data Assimilation, 38(September).

[11] H. Dastour, M.H. Bhuian, M.R. Ahmed, Q.K. Hassan, Active fire clustering and spatiotemporal dynamic models for forest fire management, Fire 7 (10) (2024) 355, https://doi.org/10.3390/fire7100355.

[12] K. Dintwe, G.S. Okin, Y. Xue, Fire-induced albedo change and surface radiative forcing in Sub-Saharan Africa savanna ecosystems: implications for the energy balance, J. Geophys. Res. Atmospheres (2017), https://doi.org/10.1002/2016jd026318.

[13] H. Eskes, A. Tsikerdekis, M. Ades, M. Alexe, A. Benedictow, Y. Bennouna, L. R. Blake, I. Bouarar, S. Chabrillat, R. Engelen, Q. Errera, J. Flemming, S. Garrigues, J. Griesfeller, V. Huijnen, L. Ilić, A. Inness, J. Kapsomenakis, Z. Kipling, V. Peuch, Technical note: evaluation of the copernicus atmosphere monitoring service Cy48R1 upgrade of June 2023, Atmos. Chem. Phys. 24 (16) (2024) 9475–9514, https://doi.org/10.5194/acp-24-9475-2024.

[14] D. Fisher, M.J. Wooster, W. Xu, G.E. Thomas, P. Lestari, Top-Down estimation of particulate matter emissions from extreme tropical peatland fires using geostationary satellite fire radiative power observations, Sensors 20 (24) (2020) 7075, https://doi.org/10.3390/s20247075.
[15] J.T. Fox, M. Vandewalle, K.A. Alexander, Land cover change in Northern Botswana: the influence of climate, fire, and elephants on Semi-Arid savanna woodlands, Land (2017), https://doi.org/10.3390/land6040073.
[16] P.H. Freeborn, M.J. Wooster, D.P. Roy, M.A. Cochrane, Quantification of MODIS fire radiative power (FRP) measurement uncertainty for use in Satellite-Based active fire characterization and biomass burning estimation, Geophys. Res. Lett. (2014), https://doi.org/10.1002/2013gl059086.
[17] Mark Friedl, D. Sulla-Menashe, MODIS/Terra+Aqua land cover type yearly L3 global 500m SIN grid V061 [Data set], NASA EOSDIS Land Process. DAAC (2022), https://doi.org/10.5067/MODIS/MCD12Q1.061.
[18] P. Friedlingstein, M. O'Sullivan, M.W. Jones, R.M. Andrew, J. Hauck, P. Landschützer, C. Le Quéré, H. Li, I.T. Luijkx, A. Olsen, G.P. Peters, W. Peters, J. Pongratz, C. Schwingshackl, S. Sitch, J.G. Canadell, P. Ciais, R.B. Jackson, S. R. Alin, J. Zeng, Global carbon budget 2024, Earth Syst. Sci. Data 17 (3) (2025) 965–1039, https://doi.org/10.5194/essd-17-965-2025.
[19] S. Garrigues, M. Ades, S. Remy, J. Flemming, Z. Kipling, I. Laszlo, M. Parrington, A. Inness, R. Ribas, L. Jones, R. Engelen, V.-H. Peuch, Impact of assimilating NOAA VIIRS aerosol optical depth (AOD) observations on global AOD analysis from the copernicus atmosphere monitoring service (CAMS), Atmos. Chem. Phys. 23 (18) (2023) 10473–10487, https://doi.org/10.5194/acp-23-10473-2023.
[20] L. Giglio, Viirs/npp active fires 6-min L2 Swath 375m V002 [Data Set], NASA Land Process. Distrib. Act. Arch. Cent. (2024), https://doi.org/10.5067/VIIRS/VNP14IMG.002. Date Accessed: 2025-08-16.
[21] L. Giglio, T. Loboda, D.P. Roy, B. Quayle, C.O. Justice, An active-fire based burned area mapping algorithm for the MODIS sensor, Remote Sens. Environ. 113 (2) (2009) 408–420, https://doi.org/10.1016/j.rse.2008.10.006.
[22] L. Giglio, W. Schroeder, C.O. Justice, The collection 6 MODIS active fire detection algorithm and fire products, Remote Sens. Environ. 178 (2016) 31–41, https://doi.org/10.1016/j.rse.2016.02.054.
[23] GMP. (2025). Factsheet: 2024 Global Methane Pledge Ministerial | Global Methane Pledge. ⟨https://www.globalmethanepledge.org/news/factsheet-2024-global-methane-pledge-ministerial⟩.
[24] S. Gonzi, P.I. Palmer, R. Paugam, M.J. Wooster, M.N. Deeter, Quantifying pyroconvective injection heights using observations of fire energy: sensitivity of spaceborne observations of carbon monoxide, Atmos. Chem. Phys. 15 (8) (2015) 4339–4355, https://doi.org/10.5194/acp-15-4339-2015.
[25] D. Griffin, J. Chen, K. Anderson, P.A. Makar, C.A. McLinden, E. Dammers, A. Fogal, Biomass burning CO emissions: exploring insights through TROPOMI-derived emissions and emission coefficients, Atmos. Chem. Phys. 24 (17) (2024) 10159–10186, https://doi.org/10.5194/acp-24-10159-2024.
[26] S. Hantson, A. Arneth, S.P. Harrison, D.I. Kelley, I. Colin Prentice, S.S. Rabin, S. Archibald, F. Mouillot, S.R. Arnold, P. Artaxo, D. Bachelet, P. Ciais, M. Forrest, P. Friedlingstein, T. Hickler, J.O. Kaplan, S. Kloster, W. Knorr, G. Lasslop, C. Yue, The status and challenge of global fire modelling, Biogeosciences 13 (11) (2016) 3359–3375, https://doi.org/10.5194/bg-13-3359-2016.
[27] C. Ichoku, African biomass burning and its atmospheric impacts. Oxford Research Encyclopedia of Climate Science, Oxford University Press, 2020, https://doi.org/10.1093/acrefore/9780190228620.013.523.
[28] C. Ichoku, L. Ellison, Global top-down smoke-aerosol emissions estimation using satellite fire radiative power measurements, Atmos. Chem. Phys. 14 (13) (2014) 6643–6667, https://doi.org/10.5194/acp-14-6643-2014.
[29] Intergovernmental Panel on Climate Change (IPCC). (2023). Climate Change 2023: Synthesis Report (H. L. Core Writing Team & J. Romero, Eds.). https://doi.org/10.59327/IPCC/AR6-9789291691647.
[30] J.W. Kaiser, A. Heil, M.O. Andreae, A. Benedetti, N. Chubarova, L. Jones, J. J. Morcrette, M. Razinger, M.G. Schultz, M. Suttie, G.R. Van Der Werf, Biomass burning emissions estimated with a global fire assimilation system based on observed fire radiative power, Biogeosciences 9 (1) (2012) 527–554, https://doi.org/10.5194/bg-9-527-2012.
[31] W. Kalisa, J. Zhang, T. Igbawua, M. Henchiri, M. Narcisse, D. Nibagwire, M. Umuhoza, Spatial and temporal heterogeneity of air pollution in east Africa, Sci. Total Environ. 886 (2023) 163734, https://doi.org/10.1016/j.scitotenv.2023.163734.
[32] C. Kloss, P. Sellitto, M. von Hobe, G. Berthet, D. Smale, G. Krysztofiak, C. Xue, C. Qiu, F. Jégou, I. Ouerghemmi, B. Legras, Australian fires 2019–2020: tropospheric and stratospheric pollution throughout the whole fire season, Front. Environ. Sci. 9 (2021), https://doi.org/10.3389/fenvs.2021.652024.
[33] S. Korontzi, Seasonal patterns in biomass burning emissions from Southern African vegetation fires for the year 2000, Glob. Change Biol. 11 (10) (2005) 1680–1700, https://doi.org/10.1111/j.1365-2486.2005.001024.x.
[34] P. Laris, Spatiotemporal problems with detecting and mapping mosaic fire regimes with coarse-resolution satellite data in savanna environments, Remote Sens. Environ. 99 (4) (2005) 412–424, https://doi.org/10.1016/j.rse.2005.09.012.
[35] Laris, P., Koné, M., Dembélé, F., Yang, L., & Jacobs, R. (2021). Methane gas emissions from savanna fires: What analysis of local burning regimes in a working West African landscape tell us. March, 1–20.
[36] C. Leisher, N. Robinson, M. Brown, D. Kujirakwinja, M.C. Schmitz, M. Wieland, D. Wilkie, Ranking the direct threats to biodiversity in Sub-Saharan Africa, Biodivers. Conserv. 31 (4) (2022) 1329–1343, https://doi.org/10.1007/s10531-022-02394-w.
[37] F. Li, X. Zhang, S. Kondragunta, Biomass burning in Africa: an investigation of fire radiative power missed by MODIS using the 375 m VIIRS active fire product, Remote Sens. 12 (10) (2020) 1561, https://doi.org/10.3390/rs12101561.
[38] Y. Liu, A. Ding, Contrasting trends of carbon emission from savanna and boreal forest fires during 1999–2022, Meteorol. Appl. 31 (1) (2024), https://doi.org/10.1002/met.2177.
[39] X. Liu, J. Ma, J. Ma, K. Chen, X. Jian, S. Tao, J. Liu, H. Gao, T. Huang, Y. Zhao, Responses of Wildfire-Induced global black carbon pollution and radiative forcing to climate change, Environ. Res. Lett. 18 (11) (2023) 114004, https://doi.org/10.1088/1748-9326/acff7a.
[40] R.L. Machete, K. Dintwe, Cyclic trends of wildfires over Sub-Saharan Africa, Fire 6 (2) (2023) 71, https://doi.org/10.3390/fire6020071.
[41] S. Martínez-Alonso, M.N. Deeter, B.C. Baier, K. McKain, H.M. Worden, T. Borsdorff, C. Sweeney, I. Aben, Evaluation of MOPITT and TROPOMI carbon monoxide retrievals using AirCore in situ vertical profiles, Atmos. Meas. Tech. 15 (16) (2022) 4751–4765, https://doi.org/10.5194/amt-15-4751-2022.
[42] J. Melo, T.R. Baker, D. Nemitz, S. Quegan, G. Ziv, Satellite-Based global maps are rarely used in forest reference levels submitted to the UNFCCC, Environ. Res. Lett. 18 (3) (2023) 034021, https://doi.org/10.1088/1748-9326/acba31.
[43] F. Mouillot, M.G. Schultz, C. Yue, P. Cadule, K. Tansey, P. Ciais, E. Chuvieco, Ten years of global burned area products from spaceborne remote sensing—A review: analysis of user needs and recommendations for future developments, Int. J. Appl. Earth Obs. Geoinf. 26 (2014) 64–79, https://doi.org/10.1016/j.jag.2013.05.014.
[44] NASA Earthdata Forum. (2024). How are Confidence Levels Classified in VIIRS Active Fires? ⟨https://forum.earthdata.nasa.gov/viewtopic.php?t=5188⟩.
[45] M. Noon, A. Goldstein, J.C. Ledezma, P.R. Roehrdanz, S.C. Cook-Patton, S. Spawn, T.M. Wright, M. González-Roglich, D.G. Hole, J. Rockström, W.R. Turner, Mapping the irrecoverable carbon in Earth's ecosystems, Nat. Sustain. 5 (1) (2021) 37–46, https://doi.org/10.1038/s41893-021-00803-6.
[46] J.J. Qi, P. Dauvergne, S. Jeudy-Hugo, J. Srouji, J.I. Allan, B. Georges-Picot, T. Evans, A. Wyns, A. Barre, D.M. Supnet, E. Maurtua Konstantinidis, A. Hammill, N. Cogswell, P. Singh, Reflections on the first global stocktake of the Paris agreement, Earth Syst. Gov. 21 (2024) 100212, https://doi.org/10.1016/j.esg.2024.100212.
[47] S. Rabin, J.R. Melton, G. Lasslop, D. Bachelet, M. Forrest, S. Hantson, J.O. Kaplan, F. Li, S. Mangeon, D.S. Ward, C. Ye, V.K. Arora, T. Hickler, S. Kloster, W. Knorr, L. Nieradzik, A. Spessa, G. Folberth, T. Sheehan, A. Arneth, The fire modeling intercomparison project (FireMIP), phase 1: experimental and analytical protocols with detailed model descriptions, Geosci. Model Dev. (2017), https://doi.org/10.5194/gmd-10-1175-2017.
[48] R. Ramo, E. Roteta, I. Bistinas, D. van Wees, A. Bastarrika, E. Chuvieco, G.R. van der Werf, African burned area and fire carbon emissions are strongly impacted by small fires undetected by coarse resolution satellite data, Proc. Natl. Acad. Sci. 118 (9) (2021) 1–7, https://doi.org/10.1073/pnas.2011160118.
[49] G.J. Roberts, M.J. Wooster, Fire detection and fire characterization over Africa using meteosat SEVIRI, IEEE Trans. Geosci. Remote Sens. 46 (4) (2008) 1200–1218, https://doi.org/10.1109/TGRS.2008.915751.
[50] G. Roberts, M.J. Wooster, W. Xu, J. He, Fire activity and fuel consumption dynamics in sub-Saharan Africa, Remote Sens. 10 (10) (2018) 1–22, https://doi.org/10.3390/rs10101591.
[51] E. Roteta, A. Bastarrika, M. Padilla, T. Storm, E. Chuvieco, Development of a Sentinel-2 burned area algorithm: generation of a small fire database for sub-Saharan Africa, Remote Sens. Environ. 222 (March) (2019) 1–17, https://doi.org/10.1016/j.rse.2018.12.011.
[52] W. Schroeder, P. Oliva, L. Giglio, I.A. Csiszar, The new VIIRS 375m active fire detection data product: algorithm description and initial assessment, Remote Sens. Environ. 143 (2014) 85–96, https://doi.org/10.1016/j.rse.2013.12.008.
[53] W. Seiler, P.J. Crutzen, Estimates of gross and net fluxes of carbon between the biosphere and the atmosphere from biomass burning, Clim. Change 2 (3) (1980) 207–247, https://doi.org/10.1007/BF00137988.
[54] G.R. Van Der Werf, J.T. Randerson, L. Giglio, T.T. Van Leeuwen, Y. Chen, B. M. Rogers, M. Mu, M.J.E. Van Marle, D.C. Morton, G.J. Collatz, R.J. Yokelson, P. S. Kasibhatla, Global fire emissions estimates during 1997-2016, Earth Syst. Sci. Data 9 (2) (2017) 697–720, https://doi.org/10.5194/essd-9-697-2017.
[55] I.R. van der Velde, G.R. van der Werf, D. van Wees, N. Schutgens, R. Vernooij, S. Houweling, E. Tonucci, E. Chuvieco, J.T. Randerson, M.M. Frey, T. Borsdorff, I. Aben, Small fires, big impact: evaluating fire emission estimates in Southern Africa using new satellite imagery of burned area and carbon monoxide, Geophys. Res. Lett. 51 (12) (2024), https://doi.org/10.1029/2023gl106122.
[56] R. Vernooij, T. Eames, J. Russell-Smith, C. Yates, R. Beatty, J.D. Evans, A. Edwards, N. Ribeiro, M.J. Wooster, T. Strydom, M. Giongo, M.A. Borges, M.M. Costa, A.C. S. Barradas, D. van Wees, G.R. van der Werf, Dynamic savanna burning emission factors based on satellite data using a machine learning approach, Earth Syst. Dyn. 14 (5) (2023) 1039–1064, https://doi.org/10.5194/esd-14-1039-2023.
[57] C. Warneke, J.P. Schwarz, J.E. Dibb, O B Калашникова, G.J. Frost, J. Al-Saad, S. S. Brown, W.A. Brewer, A.J. Soja, F.C. Seidel, R.A. Washenfelder, E.B. Wiggins, R. H. Moore, B.E. Anderson, C.E. Jordan, T.I. Yacovitch, S.C. Herndon, S. Liu, T. Kuwayama, J.H. Crawford, Fire influence on regional to global environments and air quality (FIREX-AQ), J. Geophys. Res. Atmospheres 128 (2) (2023), https://doi.org/10.1029/2022jd037758.
[58] F. Wei, S. Wang, B. Fu, M. Brandt, N. Pan, C. Wang, R. Fensholt, Nonlinear dynamics of fires in Africa over recent decades controlled by precipitation, Glob. Change Biol. (2020), https://doi.org/10.1111/gcb.15190.
[59] Wiedinmyer, C., Kimura, Y., McDonald-Buller, E.C., Emmons, L.K., Buchholz, R.R., Tang, W., Seto, K., Joseph, M.B., Barsanti, K.C., Carlton, A.G., & Yokelson, R.J. (2023). The Fire Inventory From NCAR Version 2.5: An Updated Global Fire

Emissions Model for Climate and Chemistry Applications. https://doi.org/10.5194/egusphere-2023-124.
[60] M. Wooster, Fire radiative energy for quantitative study of biomass burning: derivation from the BIRD experimental satellite and comparison to MODIS fire products, Remote Sens. Environ. 86 (1) (2003) 83–107, https://doi.org/10.1016/S0034-4257(03)00070-1.
[61] M.J. Wooster, P.H. Freeborn, S. Archibald, C. Oppenheimer, G.J. Roberts, T.E. L. Smith, N. Govender, M. Burton, I. Palumbo, Field determination of biomass burning emission ratios and factors via open-path FTIR spectroscopy and fire radiative power assessment: headfire, backfire and residual smouldering combustion in African savannahs, Atmos. Chem. Phys. 11 (22) (2011) 11591–11615, https://doi.org/10.5194/acp-11-11591-2011.
[62] M.J Wooster, G. Roberts, G.L.W Perry, Y.J Kaufman, Retrieval of biomass combustion rates and totals from fire radiative power observations: FRP derivation and calibration relationships between biomass consumption and fire radiative energy release, J. Geophys. Res.: Atmos. 110 (24) (2005), https://doi.org/10.1029/2005jd006318.
[63] J. Zhao, C. Yue, J. Wang, S. Hantson, X. Wang, B. He, G. Li, L. Wang, H. Zhao, S. Luyssaert, Forest fire size amplifies postfire land surface warming, Nature 633 (8031) (2024) 828–834, https://doi.org/10.1038/s41586-024-07918-8.
[64] B. Zheng, P. Ciais, F. Chevallier, E. Chuvieco, Y. Chen, H. Yang, Increasing forest fire emissions despite the decline in global burned area, Sci. Adv. 7 (39) (2021), https://doi.org/10.1126/sciadv.abh2646.
[65] M. Zubkova, L. Boschetti, J.T. Abatzoglou, L. Giglio, Changes in fire activity in Africa from 2002 to 2016 and their potential drivers, Geophys. Res. Lett. 46 (13) (2019) 7643–7653, https://doi.org/10.1029/2019GL083469.